Readiness Review Documentation for E-02-103 – A Precision Measurement of the Neutral Pion Lifetime via the Primakoff Effect

the *PrimEx* Collaboration

November 20, 2003

Contents

1 Proposed Agenda – November 20, 2003 **5**

2 Summary of Accomplishments and Technical Readiness **6**

3 The Hybrid Calorimeter - HYCAL **6**
3.1 Lead Glass Detectors . . . 9
3.2 Beam Test Results for the Lead Tungstate Detectors . . . 10
3.3 Energy Resolution . . . 12
3.4 Position Resolution . . . 13
3.5 Gain Change *versus* Radiation Dose Rate . . . 14
3.6 Beam Test Studies of the Lead Tungstate - Lead Glass Transition Region . . . 16
3.7 The Calorimeter Frame and Transporter . . . 18
3.8 HYCAL Gain Monitoring System . . . 19
3.9 Veto Scintillators . . . 23

4 Luminosity **24**
4.1 The Tagged Photon System . . . 24
4.2 Absolute calibration with total absorption counter . . . 26
4.2.1 Total absorption counter status . . . 27
4.3 Relative calibration with pair spectrometer . . . 27
4.4 Results from August 2002 Test Run . . . 29
4.5 Electron counting by sampling method . . . 36
4.6 Target thickness measurements . . . 38
4.7 Normalizing Primakoff yield to Compton yield . . . 39
4.8 Plans for a future luminosity beam test . . . 42

5 Data Acquisition and Electronics **42**
5.1 Electronics Overview . . . 42
5.1.1 Crates and Modules . . . 42
5.1.2 Cabling . . . 43
5.2 Event Triggers . . . 44
5.2.1 π^o trigger . . . 44
5.2.2 PS trigger . . . 44
5.2.3 LMS trigger . . . 46
5.2.4 Clock (luminosity) trigger . . . 46
5.2.5 Trigger Rates . . . 46
5.2.6 Monte Carlo Trigger Studies . . . 47
5.3 Data Format and Data Rates . . . 47
5.3.1 Data Format . . . 47
5.3.2 Data Rates/Event Sizes . . . 53
5.4 Analysis Software . . . 53
5.4.1 Object Framework . . . 53
5.4.2 Bank Definitions (BDML) . . . 53

5.5 Online Monitoring Software 53
5.5.1 ET system 53
5.5.2 Monitoring Programs 54
5.5.3 PrimEx Event Viewer (pev) 54
5.6 DAQ and Electronics Summary 55

6 Beamline instrumentation **55**
6.1 Electron beam position monitors 55
6.2 Harp 55
6.3 Online scintillating fiber based position monitor 55
6.4 Slow Controls 56

7 Calibrations via Compton Scattering **57**
7.1 Energy Calibration 57
7.2 Calibration of PrimEx setup 59

8 Summary **59**

9 Appendix I: Engineering **60**

10 Appendix II: Technical Details of Pair Spectrometer **62**
10.1 Detectors 62
10.2 Results from Magnet Mapping 63

Abstract

The PrimEx (Primakoff Experiment) Collaboration is preparing to perform a high precision (1.4%) measurement of the two photon decay width of the neutral pion, $\Gamma_{\pi^o \to \gamma\gamma}$. Photons from the Hall B photon tagging facility will be used to produce neutral pions in the Coulomb field of nuclei. The two photons from the pion decay will be detected in a hybrid calorimeter (HYCAL) which will utilize lead tungstate ($PbWO_4$) scintillating crystals as well as lead glass Cherenkov shower counters. In addition to the development of this state-of-the-art calorimeter detector, a major experimental challenge in this measurement involves control of the luminosity. Extensive studies of the photoproduction targets have been performed, and a pair production luminosity monitor, which is now a part of the standard beamline in Hall B, has been constructed and commissioned. Here, we discuss the overall readiness status of this experiment.

1 Proposed Agenda – November 20, 2003

8:45-9:00	Presentation of the charge	Volker Burkert
9:00-9:20	Overview	Ashot Gasparian
9:20-9:45	HYCAL	Ashot Gasparian
9:45-10:00	Gain Monitoring System	Samuel Danagoulian
10:00-10:10	Veto Detector	Rory Miskimen
10:10-10:30	Coffee	
10:30-11:05	Safety, Engineering and Infrastructure	Dave Kashy
11:05-11:25	Target Thickness	Rory Miskimen
11:25-11:50	Photon Flux	Dan Dale
11:50-12:20	Lunch, on your own	
12:20-13:30	Optional tour of *PrimEx* experimental equipment (Test Lab and Hall B)	
13:30-14:10	Electronics, DAQ, Online Analysis, Rates, Beam Backgrounds	David Lawrence
14:10-14:20	Slow Controls	A. Ahmidouch
14:20-14:35	Beamline	Dustin McNulty
14:35-14:55	Calibrations with Compton Scattering: Photon Energy and Overall Setup	Liping Gan
14:55-15:15	Coffee	
15:15-15:40	Schedule and Summary	Ashot Gasparian
15:40	Executive session and close-out	

2 Summary of Accomplishments and Technical Readiness

The primary experimental equipment required in this experiment includes: (1) the Hall B photon tagger; (2) 5% radiation length solid π^o production targets (^{12}C, ^{120}Sn, and ^{208}Pb); (3) a pair production luminosity monitor located just downstream of the π^o production target; (4) a 1m $\times$ 1m highly segmented lead glass photon detector for π^o decay photons with a high resolution insertion in the central region near the beam, and a plastic scintillator charged particle veto. (See figure 1.) Significant recent milestones include:

- Pair spectrometer installed and commissioned.
- HYCAL transporter assembled and in final stages of testing.
- All lead tungstate and lead glass modules assembled and stacked in frame.
- Approximately 2000 high voltage dividers constructed and tested with PMT's.
- Installation of all PMT's in HYCAL complete.
- Cosmic ray tests will start week of December 1^{st} in Test Lab with full *PrimEx* electronics and DAQ.

3 The Hybrid Calorimeter - HYCAL

At the incident photon energies of this experiment ($E_\gamma = 4.6 - 5.7$ GeV), the Primakoff cross section peaks at extremely small angles. For instance at $E_\gamma = 5$ GeV, $\theta_{peak} = 0.02^o$. In order to identify and extract the Primakoff amplitude, the experimental setup must have sufficient angular resolution for forward pion production. Both photons from the $\pi^o \to \gamma\gamma$ decay will be detected in the electromagnetic hybrid calorimeter (HYCAL). Therefore the pion angular resolution will depend strongly on the position and energy measurement accuracy of the calorimeter. Implementation of the photon tagging technique will, in addition to photon flux control, provide information on the initial photon energy at the level of 10^{-3}. This knowledge of the initial photon energy will apply a kinematical constraint to this two body reaction and provide about a 30% improvement in the angular resolution[1]. We have constructed a multichannel hybrid calorimeter which consists of two types of shower detectors: lead glass Cherenkov modules located on the peripheral part of the calorimeter, and lead tungstate scintillating crystals in the central region, with a hole in the middle for the passage of the photon beam through the calorimeter. This design is based on an optimization of the cost and performance of the calorimeter. The $PbWO_4$ crystals are half the size of the lead glass Cherenkov radiators, and provide energy and position resolutions which are approximately twice better. On the other hand, the price per unit area of detector is approximately 4-5 times higher for the crystal detectors as compared to lead glass. The transverse dimensions of the HYCAL calorimeter (116 x 116cm^2) were chosen to have sufficient geometrical efficiency with the fixed central hole ($4\times4cm^2$) in the middle of the detector. At a distance of 7.5 m

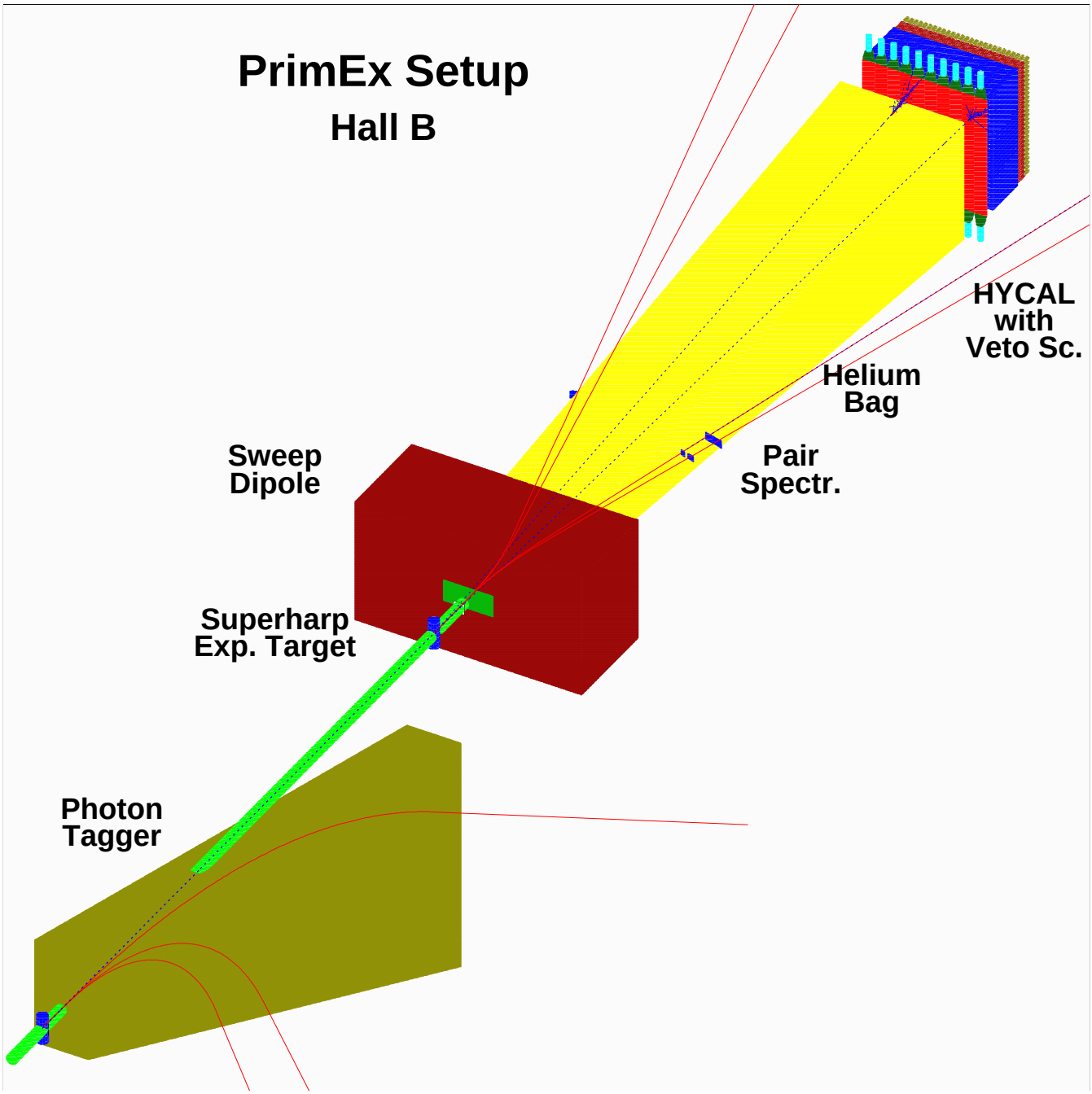

Figure 1: Layout of the experimental setup.

from the production target, the designed setup has about a 70% geometrical acceptance for the forward going neutral pions.

We have performed two beam tests for the prototype detectors including crystals from the two major manufacturers – Bogoroditsk Techno-Chemical Plant (BTCP), Bogoroditsk, Russia and the Shanghai Institute of Ceramics (SIC), Shanghai, China. In addition, we have performed studies of their mechanical and optical properties. Figure 2 shows the transmission as a function of wavelength, measured at Jefferson Lab, for two types of crystals. The energy and position resolutions as well as the effect of the rate dependence of the light yield for both types of crystals for a few GeV electron beam were also measured. The results of these tests are described below. We chose to purchase the crystals from SIC based on the high performance they exhibited in these tests as well as the comparatively lower price which we were able to obtain through our Chinese collaborators. This has enabled us to increase the number of crystals in the calorimeter by more than a factor of two over that envisioned in the original proposal, and thereby enhance its high resolution capabilities. The HYCAL now consists of 1152 $PbWO_4$ crystals which cover the 70×70 cm^2 central part of the calorimeter.

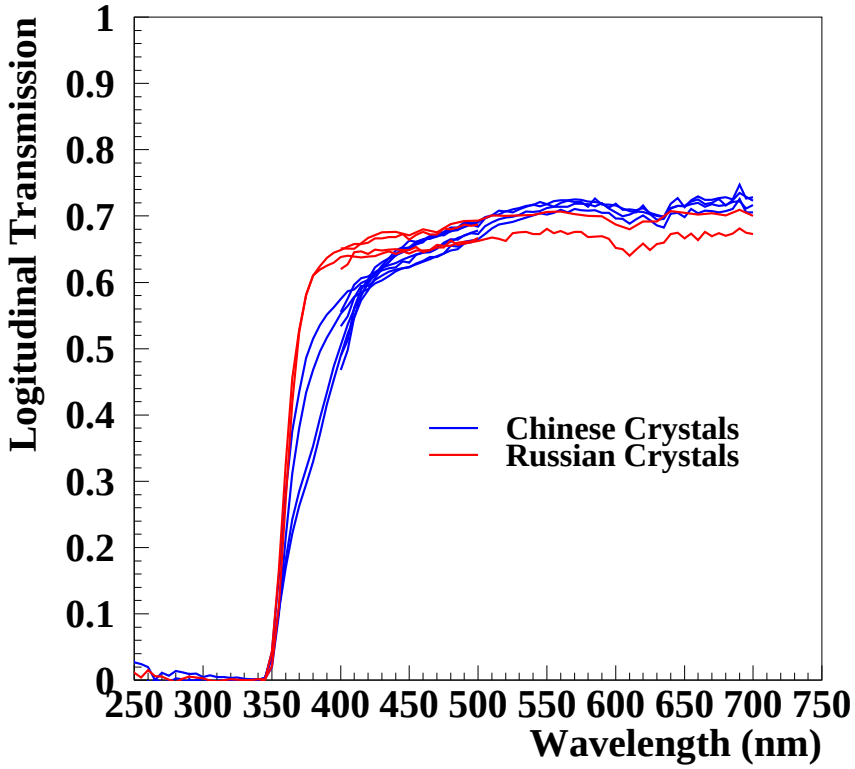

Figure 2: Transmission as a function of wavelength for lead tungstate crystals.

All detector modules of the calorimeter have been assembled and stacked in their frame in the Test Laboratory. A photograph of the assembled detector is shown in figure 3. During data taking, the calorimeter will be calibrated with tagged photon beams to determine the

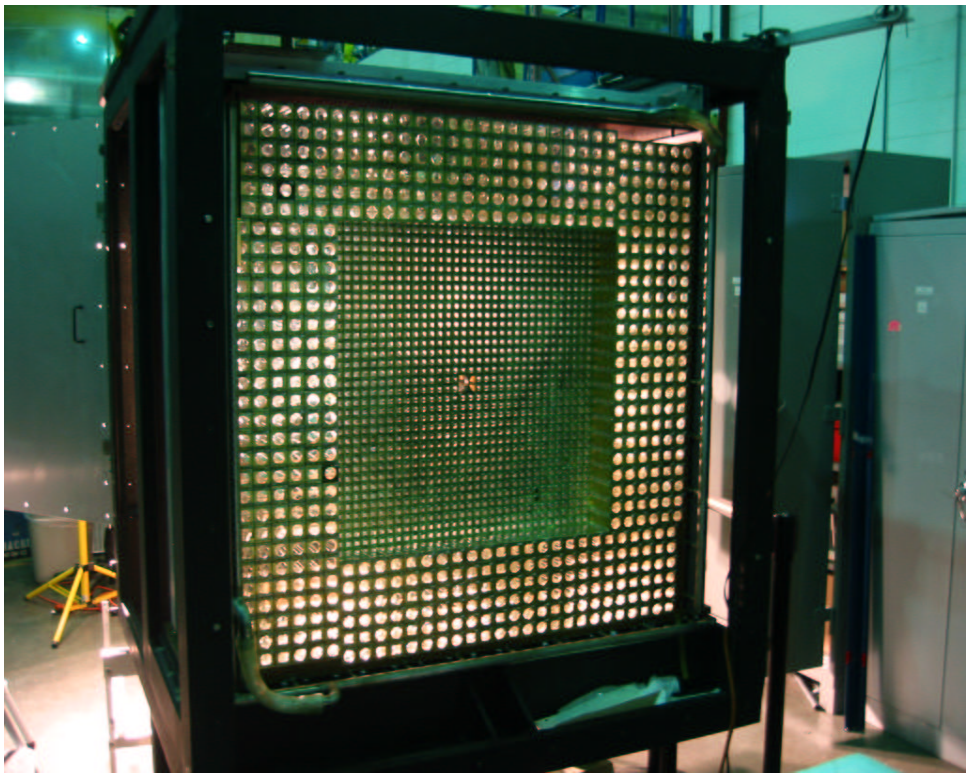

Figure 3: The Hybrid Calorimeter in the Test Lab with all detector elements stacked.

gains of the counters. For this purpose, the calorimeter will be installed on a transporter allowing every counter of the detector to be centered on the beam. To monitor and correct possible gain changes between beam calibrations, a light monitoring system will be used.

3.1 Lead Glass Detectors

Two institutions from Russia which have provided lead glass detectors for the HYCAL calorimeter are involved in the collaboration–the Institute for Theoretical and Experimental Physics (ITEP), Moscow and the Institute for High Energy Physics (IHEP), Protvino. We have done several beam tests to define the best lead glass detectors for this experiment. The main considerations have been to optimize the detection efficiency as well as the energy and position resolutions for few GeV photons. The results for the energy and position resolution in the few GeV range, as measured by a prototype detector which we have constructed, are shown in figures 4 and 5. Based on these test results, we selected TF-1 type lead glass modules with dimensions $3.8\times3.8\times45cm^3$. These have been assembled and stacked in the detector frame.

In figure 6, a fully assembled lead glass counter is shown before being installed in the detector array. Cherenkov light produced in the lead glass radiator from the electromagnetic shower will be detected by a photomultiplier tube (FEU-84-3, made in Russia). The individual blocks are wrapped in $25\mu m$ aluminized mylar foil which serves as a light reflector and

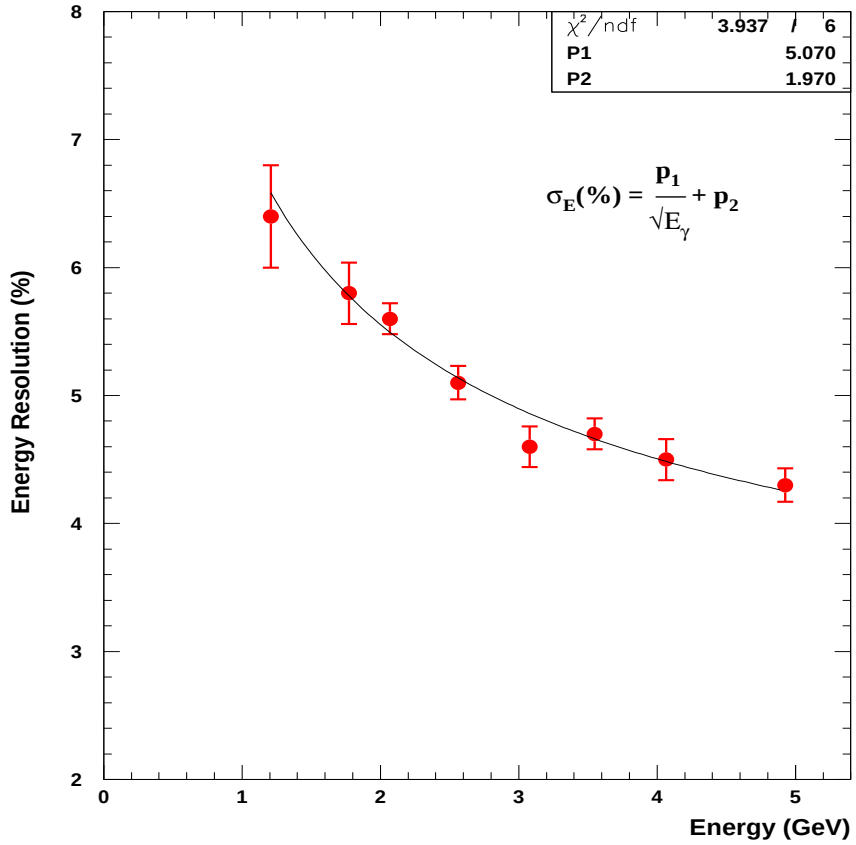

Figure 4: The prototype lead glass detector energy resolution.

an optical isolator between the blocks. The mechanical assembly of each module consists of two brass flanges which are kept together by $25\mu m$ thick stressed brass strips.

3.2 Beam Test Results for the Lead Tungstate Detectors

Because of its fast decay time, high density, and high radiation hardness, lead tungstate ($PbWO_4$) has become a popular inorganic scintillator material for precision compact electromagnetic calorimeters in high energy physics experiments (CMS, ALICE for LHC) in the past decade. There are two major commercial suppliers of $PbWO_4$ crystals: the BTCP factory in Bogoroditsk, Russia, and SIC, in Shanghai, China. In order to check the performance of the crystals with few GeV electron/photon beams and also to select the manufacturer for the HYCAL calorimeter, we performed two beam tests with a prototype crystal detector. A matrix consisting of 6×6 $PbWO_4$ crystals was stacked in a light tight aluminum frame which could be cooled down to a well stabilized temperature (T = $4°C$ for these tests). The light yield of the crystal is highly temperature dependent ($\sim 2\%/°C$ at room temperature). Therefore one of the technical challenges for this detector is to reach high stabilization of the crystal temperature during the experiment. In order to accomplish this, the crystal assembly

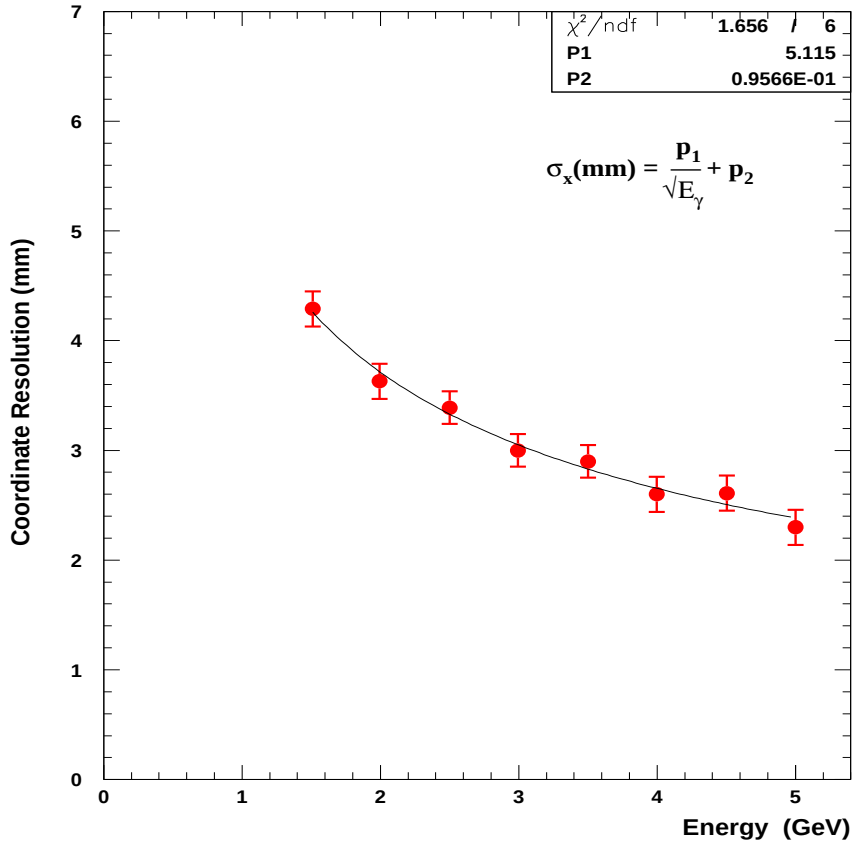

Figure 5: The prototype lead glass detector coordinate resolution.

was surrounded by massive copper plates with water circulating through pipes. Six of the crystals were equipped with temperature sensors on their front faces and read out by computer during the beam test measurements. In figure 7, we show the temperature stability for several crystals during twelve hours of data taking in a tagged photon beam. As can be seen from the plot, the temperature in the prototype calorimeter was stabilized at the level of $\pm 0.1^{\circ}C$.

The upper 3×6 section of the detector was assembled from crystals made in Russia, and the bottom section consists of Chinese crystals from SIC. The scintillation light from the electromagnetic shower was detected with Hamamatsu R4125HA photomultiplier tubes coupled to the back of the crystals with optical grease. Individual crystals were wrapped in $100\mu m$ TYVEK. The photomultiplier tubes were attached to the crystals with two specially designed brass flanges attached to the front and back of the crystals. These brass pieces are kept together by two stretched $25\mu m$ thick brass strips as can be seen in figure 8.

We moved the prototype detector by remote control in two dimensions perpendicular to the secondary electrons, which were selected by the PrimEx/Hall B dipole magnet and the scintillating telescopes. A x and y coordinate scintillation fiber detector (2 mm in fiber

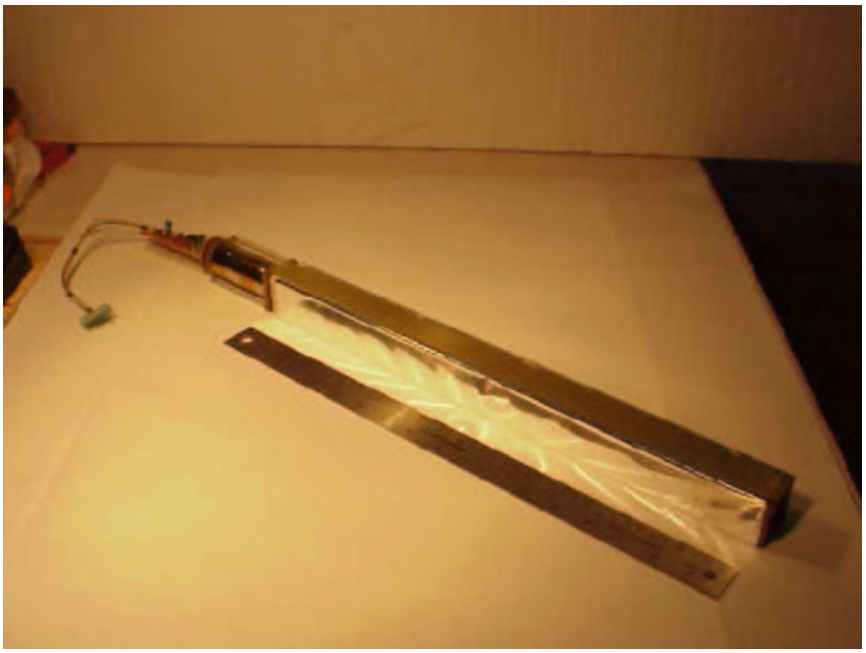

Figure 6: A lead glass detector module.

size) was used on the front of the detector to define the impact points of the electrons. The anode output from each photomultiplier tube was digitized by means of a 14-bit charge-sensitive ADC (LeCroy 1881M, integration width = 200 nsec). The performance of the crystal prototype was studied with secondary electrons with energy $E_e = 2$ and 4 GeV.

3.3 Energy Resolution

The calibration of the calorimeter was performed with 4 GeV electrons by irradiating the centers of each crystal module with a narrow electron beam defined by 2×2 scintillating fiber elements (4×4 mm in size). Then to measure the energy resolution, the centers of both the SIC and BTCP crystal arrays were irradiated with sufficient statistics. We have found a slightly better energy resolution for the SIC crystals. We attribute this to their relatively higher ($\sim$ 20%) light yield. For the final energy and position resolution, the central part of the prototype detector was irradiated with 2 and 4 GeV electrons. The reconstructed energy distribution for the 4 GeV electrons is shown in figure 9 for three different calibrated ADC sums: the central module; the inner section comprising 3×3 crystals and the total array of 6×6 crystals. The energy resolution is obtained using a Gaussian fit of the 6×6 distribution. As can be seen in the figure, an excellent energy resolution of $\sigma_E/E = 1.3\%$

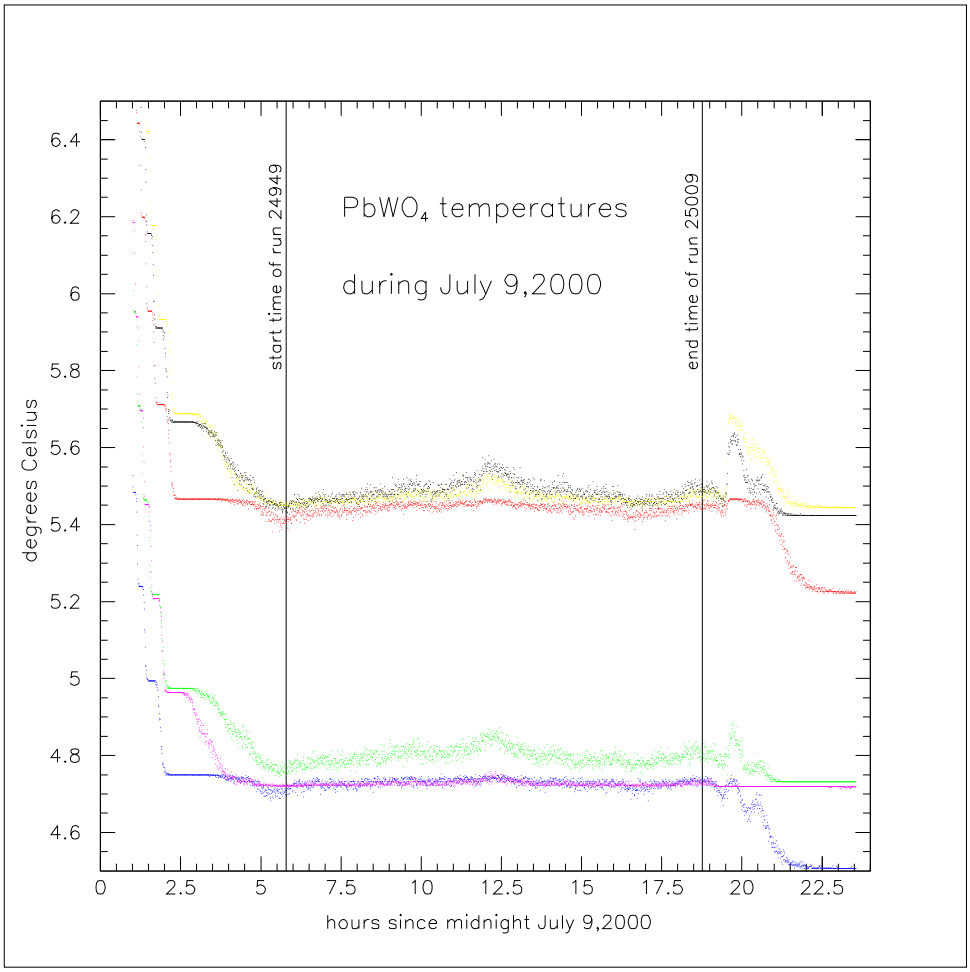

Figure 7: The temperature stability of the lead tungstate crystals during a twelve hour period.

has been achieved for 4 GeV electrons. After subtraction of the beam energy spread due to the finite size of the scintillator fibers as well as multiple scattering effects, this resolution reaches the 1.2% level.

3.4 Position Resolution

An important requirement for the HYCAL is the accuracy of the reconstructed position for the decay photons. The impact position of the photons will be determined from the energy of the electromagnetic shower deposited in several neighboring counters. In the case of the $PbWO_4$ crystals, the transverse size of the shower is about two times smaller than that in lead glass. As a result, the position resolution in the $PbWO_4$ detector with an optimal cell size should be two times smaller than lead glass detectors. To maximize the position resolution, we have optimized the crystals' transverse dimension, and have selected it to be $2.05 \times 2.05\ cm^2$. This size is comparable to the Molière radius of the crystal material. The distribution of the reconstructed coordinates for the 4 GeV electrons hitting a crystal cell boundary is shown in figure 10. The linear dependence of the reconstructed coordinates obtained from a logarithmically weighted average of the cell signals, *versus* the impact positions determined by the fiber scintillator detectors is shown in figure 11. As is well known,

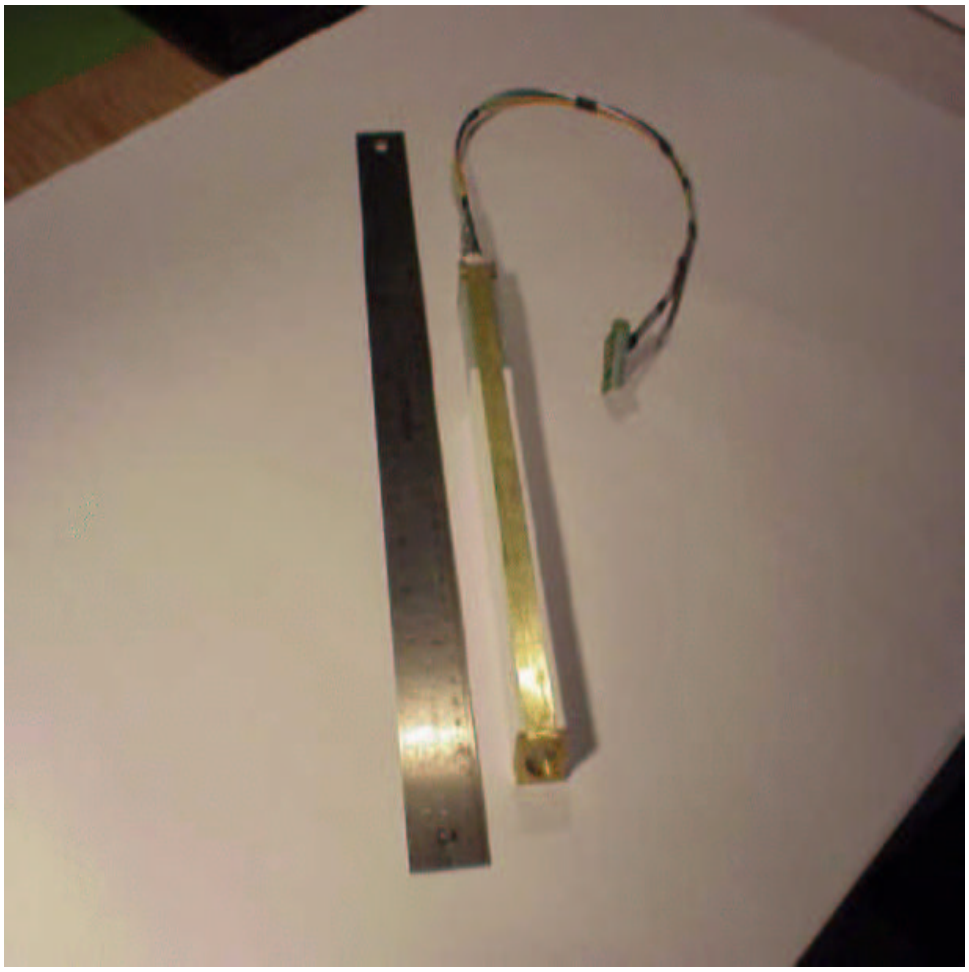

Figure 8: A lead tungstate detector module.

there is a rather strong correlation between the position resolution (σ_x) and the point at which the incoming electrons (or photons) hit the detector face. The top plot of the figure shows this dependence for the $PbWO_4$ crystal detectors as obtained from our beam tests. σ_x is smaller (1.28 mm) near the edge of the cell and rises to 2.1 mm in the cell center. These tests showed no measurable difference in the coordinate resolution for the two types of crystals produced by SIC and BTCP.

3.5 Gain Change *versus* Radiation Dose Rate

It is well known that all types of crystal scintillators are sensitive to radiation. Because of their fast decay time and high density, $PbWO_4$ crystals were first chosen for use in the CMS and ALICE experiments to construct high precision electromagnetic calorimeters at LHC[2]. The integral radiation level for the CMS experiment is about two orders of magnitude higher than that of the central part of the HYCAL crystal detectors for the PrimEx experiment. For our experiment, the more important characteristic is the change in the crystal response due the radiation dose rate. It was observed experimentally for the earlier crystals that even for a small dose rate ($\sim$ 1 Rad/hour), the gain changes were at the few per cent level. It

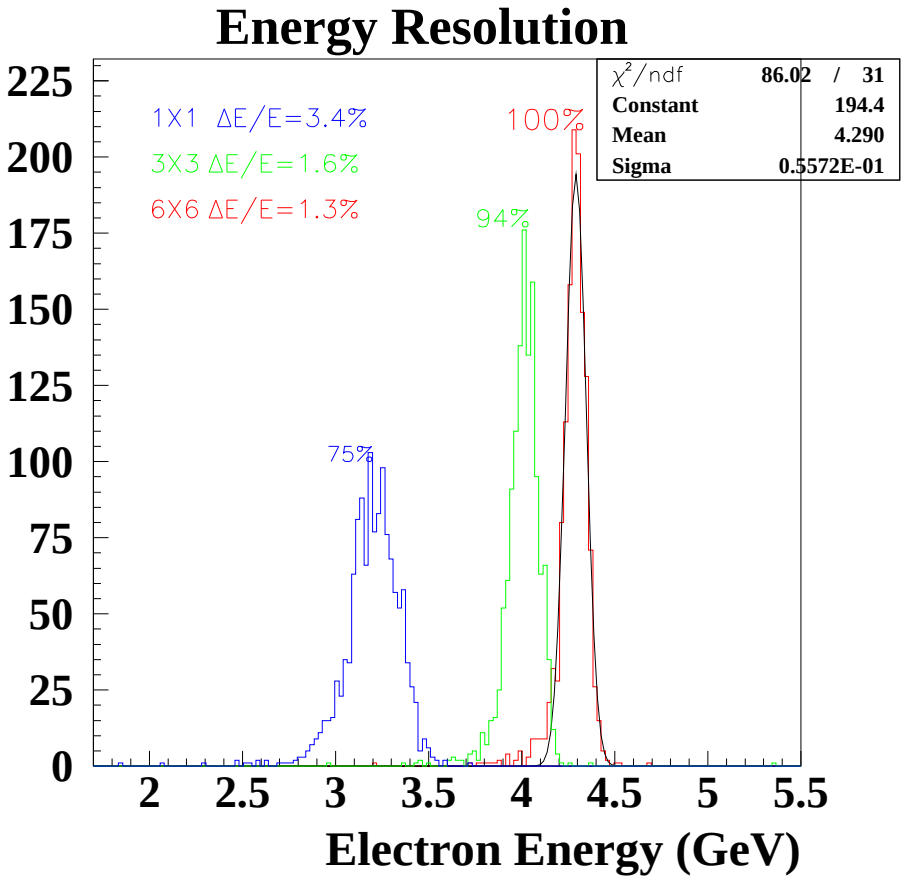

Figure 9: Energy response of a $PbWO_4$ crystal array to 4 GeV electrons. Left peak: single crystal; center peak: 3×3 array; right peak: 6×6 array.

was understood that this effect is not a result of the change of scintillation mechanism of the material, but the loss of light output due only to absorption by radiation-induced color centers[3]. This effect has been shown to be clearly correlated with the crystal annealing conditions. A dramatic improvement of this effect has been achieved in recent years by both of the commercial crystal producers. We have done experimental studies of this for each of the two types of crystals produced in the past two years in Russia and China. For these tests, several crystal centers were irradiated with a 4 GeV electron beam at different rates. The duration of each irradiation was kept to about 20 to 30 minutes. The ADC information from all channels of the 6×6 matrix prototype was recorded continuously during the beam irradiation. The normalized pulse height for three typical crystal detectors from each manufacturer is plotted *versus* the relative beam rate in figure 12. The statistical error for each point is shown, and is much bigger for the lower rates for obvious reasons. The plot shows the relative pulse heights as a function of rate for 4 GeV electrons normalized to the 5 kHz point. As is evident from these measurements, we observe opposite behavior for the two types of crystals at high rates. The gain change could be caused by three different

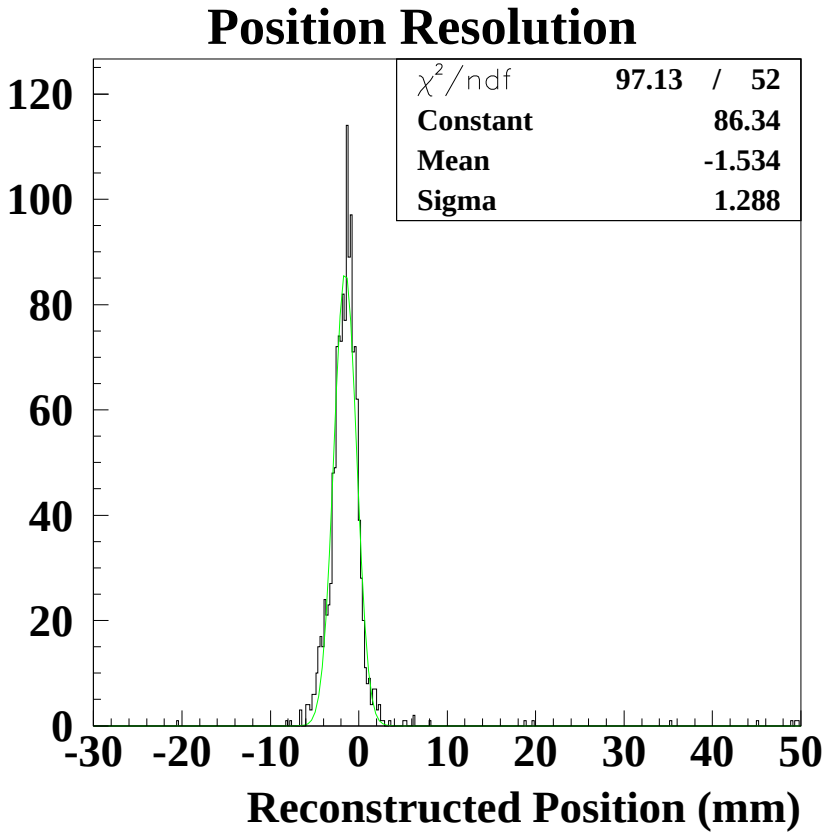

Figure 10: Distribution of reconstructed positions at the boundary between two lead tungstate crystal detectors.

effects: (1) the change of the scintillation mechanism in the crystal; (2) the change in the light collection in the radiator; and (3) PMT gain change *versus* rate. Our Monte Carlo calculations show that the PrimEx dose rate in the experiment will be equivalent to 10 kHz for 1 GeV electrons or photons. This is twice less than the dose rate for the 5 kHz at 4 GeV point shown on the plot. These rate studies show that both types of crystals can be used for the HYCAL calorimeter in the PrimEx experiment.

3.6 Beam Test Studies of the Lead Tungstate - Lead Glass Transition Region

The hybrid nature of the *PrimEx* HYCAL calorimeter arises from the optimization of performance *versus* cost. In August 2002, beam test studies were performed which focused on the properties of the detector response in the transition region between the two types of shower detector modules. A combined matrix of detectors consisting of 96 lead glass and 77 lead tungstate modules was constructed and is shown in figure 13. The detector geometry

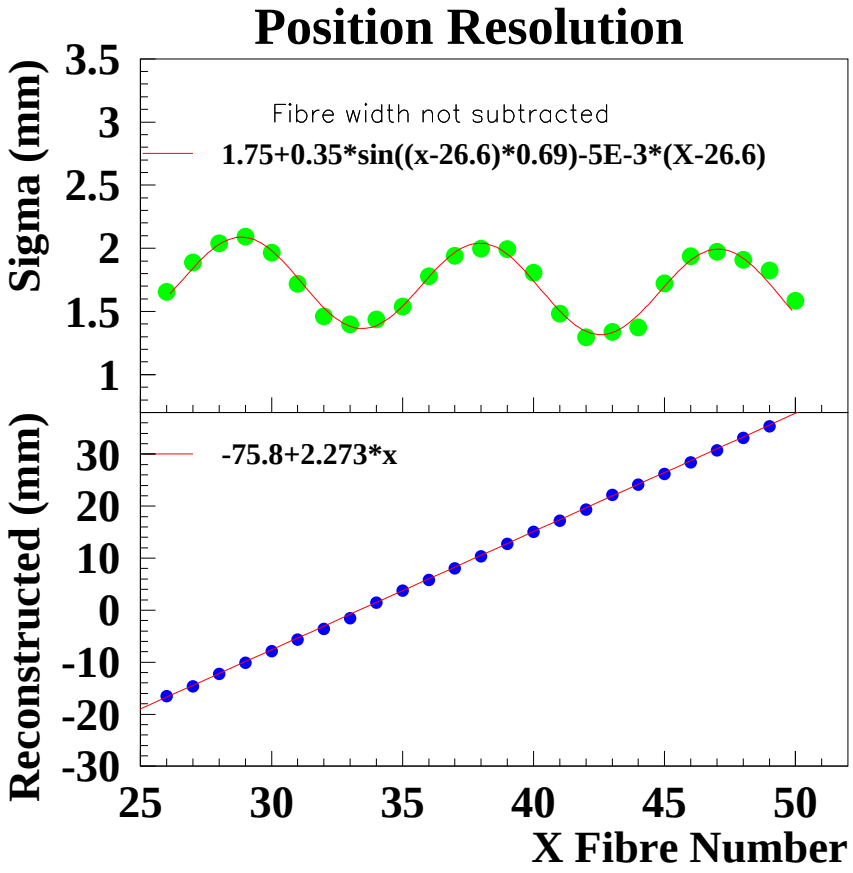

Figure 11: Position resolution (top) and reconstructed *versus* actual position (bottom) across the face of a $PbWO_4$ crystal array.

was such that the lead tungstate modules were shifted downstream of the lead glass modules by seven centimeters to minimize shower leakage out of the uncovered back and sides of the lead glass blocks. (Detailed investigations of this issue can be found in reference [14]).

A tagged photon beam of energy $3.7 < E_\gamma < 4.4GeV$ was scanned across the boundary, and the energy resolution of the shower cluster was determined as a function of position. The results are shown in figure 14 (top), where the degradation in resolution as one goes from lead tungstate to lead glass is evident. This effect is well described by the Monte Carlo simulation (blue band) performed for $E_\gamma = 4.0GeV$. Figure 14 (bottom) shows the relative reconstructed energy as a function of position, where the dip at the interface predominantly arises from shower leakage from the uncovered backs and sides of the lead glass blocks. This effect is governed by the different radiative lengths of the two types of detector materials ($R_{PbWO_4} = 0.89cm$ and $R_{\rm leadglass} = 2.75cm$, thus requiring the lead tungstate modules to be physically shorter), as well as their relative offsets (the front faces of the lead tungstate modules were 7 cm downstream of those of the lead glass). Since we had very limited beam time for the HYCAL0 tests, these data for the transition region are not yet complete. We

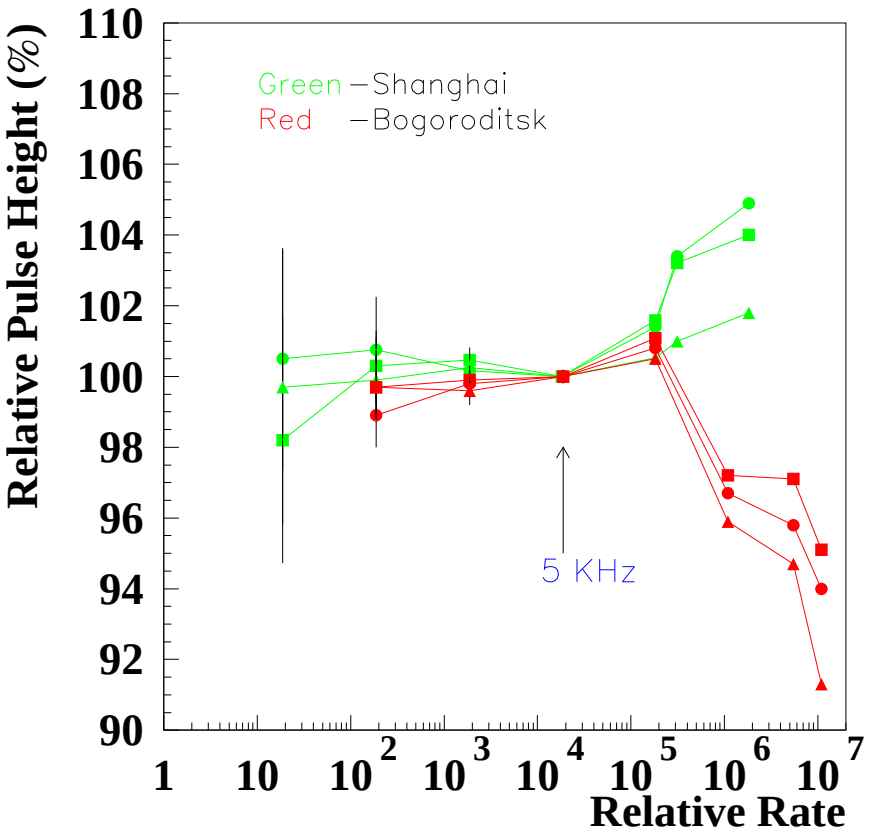

Figure 12: Relative pulse height *versus* rate for Chinese and Russian $PbWO_4$ crystals.

are planning to map this region of the HYCAL in detail during commissioning, and thereby determine the fiducial acceptance of the detector with the required precision.

3.7 The Calorimeter Frame and Transporter

The individual modules of the HYCAL are assembled in a rectangular box inside of the calorimeter frame. The entire assembly weighs over five tons, and is movable in both horizontal and vertical directions in order to place each module in the beam for energy calibration. The transporter, shown in figure 3.6, has been designed and constructed to provide movement of the entire assembly of detectors, its support frame, the thermo-stabilization system, and the delay cables. The light monitoring system will also be mounted on top of the HYCAL frame.

A drawing of the calorimeter in the data taking position is shown in figure 16. In this configuration, the accuracy of centering the detector transverse to the beam will be $\pm 0.7mm$. The calorimeter will be remotely movable so that during calibration, each module can be positioned in the beam of tagged photons with an accuracy of $\pm 2mm$. The system also

Figure 13: The prototype hybrid calorimeter HYCAL0 (left), and Hall B engineer Dave Kashy (rught).

provides the capability to move the detector along the beamline. The conceptual design for this system is shown in figure 17.

When the calorimeter is not being used in the beam, the transporter system will provide positioning of the entire calorimeter a few meters above the beam center on Level 2 of the Hall B Space Frame. In addition to storage, this configuration will allow the HYCAL to be available for assembly, maintenance, and testing with cosmic rays. This design has the advantages of maximizing experimenters' access to the detector while minimizing impact on other Hall B operations.

3.8 HYCAL Gain Monitoring System

The main components of the Light Monitoring System (LMS) are: (1)a light source, (2) a mixing box, (3) a light distribution system, (4)filter wheel, (5)reference detectors and (5) a dedicated computer for data acquisition system. The optical components and the reference detectors are mounted in a thermally insulated box whose temperature is controlled at a level of 0.1°C.

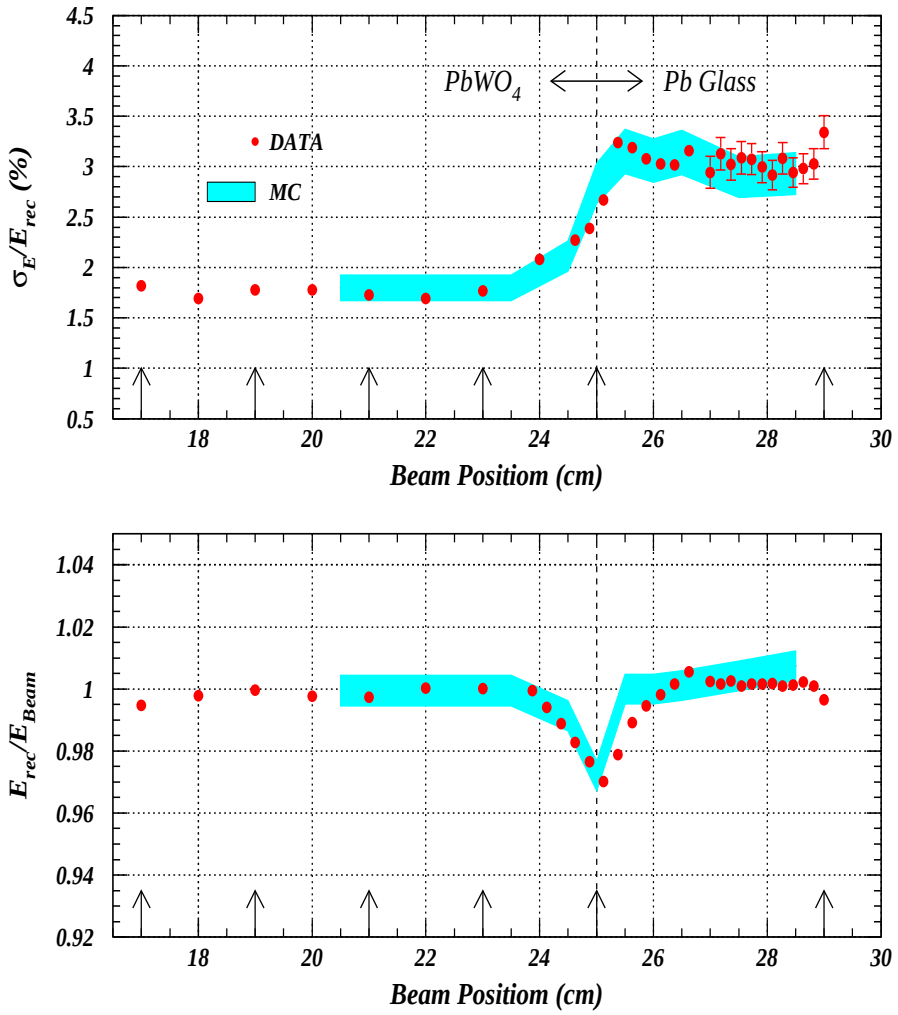

Figure 14: Preliminary results of beam test studies of the transition region between $PbWO_4$ and lead glass detector modules. Top: energy resolution of the shower clusters. Bottom: relative reconstructed energy *versus* position. In both cases the blue bands indicate Monte Carlo simulations.

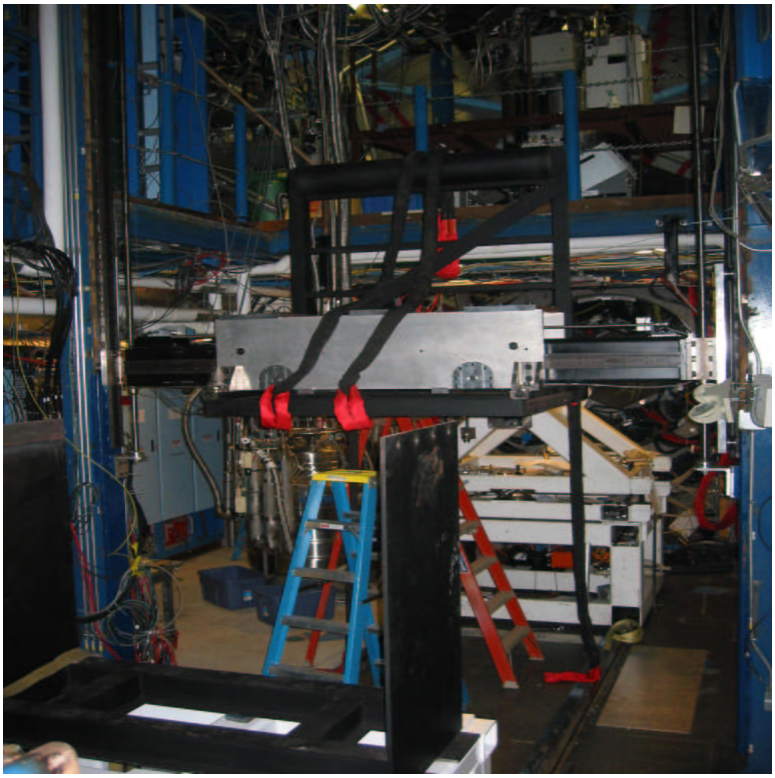

Figure 15: The HYCAL transporter in Hall B.

The Light Source

The light source comprises an assembly of 31 NICHIA super bright blue LEDs (peak wavelength 470 nm) connected in series. The LED assembly is powered by 150 V, 8 nsec pulses generated in a circuit, based on a transistor in avalanche mode. The width of the light pulse is on the order of 35 nsec (FWHM) at the output. The fluctuations of the intensity of the light pulse during a week period remains within $(1. - 1.5)\%$. Pulse fluctuations over the period of one measurement (2 to 5 min) is on the order of 0.2% on average. The prototype light source has been continuously powered during twelve consecutive months and no noticeable degradation of the performance has been observed.

Light Mixing and Distribution

For light mixing, a six inch diameter integrating sphere is being utilized. Light is distributed to the individual calorimeter modules via a bundle of silica-glass fibers with the highest radiation hardness. The length of the fibers is 3m, and the diameter of the core is 200 μm. Each fiber from the bundle is terminated on the detector end by a plastic ferrule 5 mm in height and 4.6 mm in diameter, with a central hole for the fiber. The ferrule is glued to the front face of the detector module with soft UV glue. This provides a moisture free soft interface. There is a filter wheel between the integrating sphere and the bundle. Light from LMS will be periodically injected into the detector modules between real events during data taking with a frequency between 10 and 20 Hz.

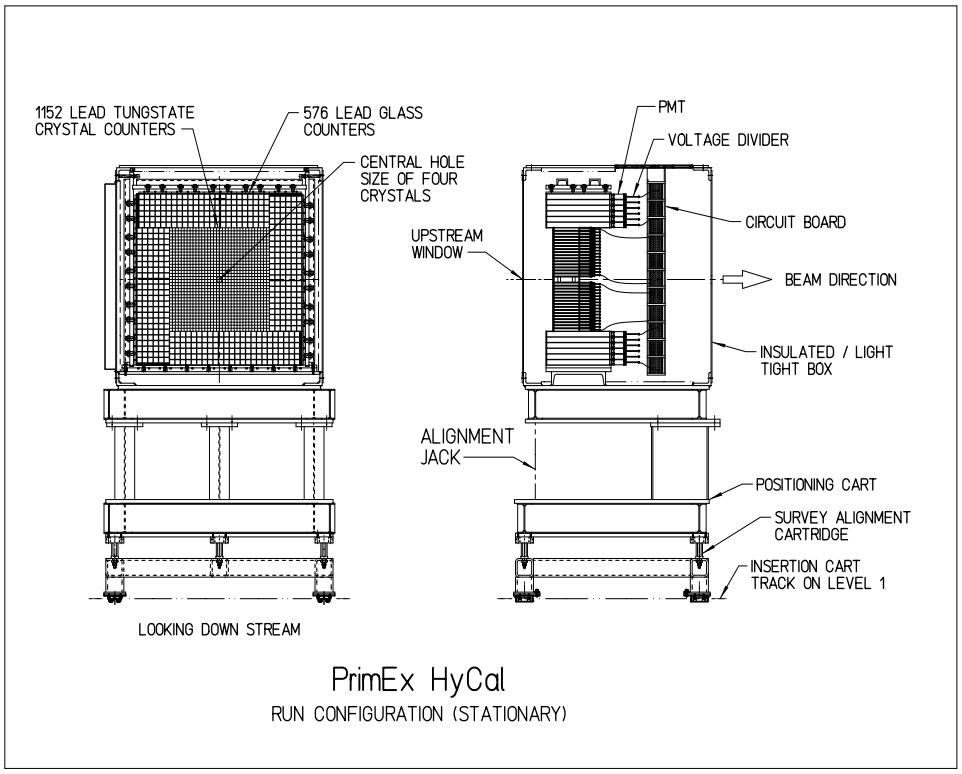

Figure 16: The HYCAL detector on its support stand in the run configuration.

Reference Detectors

For reference detectors we use a P/N photodiode with an amplifier, connected directly to the integrating sphere, and three photomultiplier tubes (Hamamatsu, 2" diameter). The light pulse is transmitted to the reference PMT via fiber cables from the bundle. Each reference PMT is provided with a radioactive α-source (Am^{241}) on a scintillating YAP crystal.

Data Acquisition

A CAMAC based Data Acquisition System with LabView DAQ software is being used for readout and on-line analysis. A reference point will be generated every 2-3 minutes through an EPICS variable.

Results of the Stability Test

A long term stability test of the prototype LMS as well as beam test, have been performed during July-August 2002, when HYCAL-0 was mounted on the beam line. The results are presented in this section. For this test, the light intensity has been monitored with a PIN photodiode and three reference PMTs. In figure 18, top picture, the distribution of the ratio, PMT_1/PMT_3, for the period of time of 540 hours is shown. The same ratio plotted versus time, is presented in the bottom picture.

The preliminary results of the beam test from August 30, 2002, are presented in figure 19. In this test, the high voltage of the PMT of one of HYCAL-0 modules (the central module from the group of 3x3 crystals) with the photon beam on it, has been varied between 1170 and 1200 V. The initial calibration of the calorimeter module was done with the PMT high voltage at 1200 V. The modified calibration curves (at 1170 and 1190 V) have been corrected

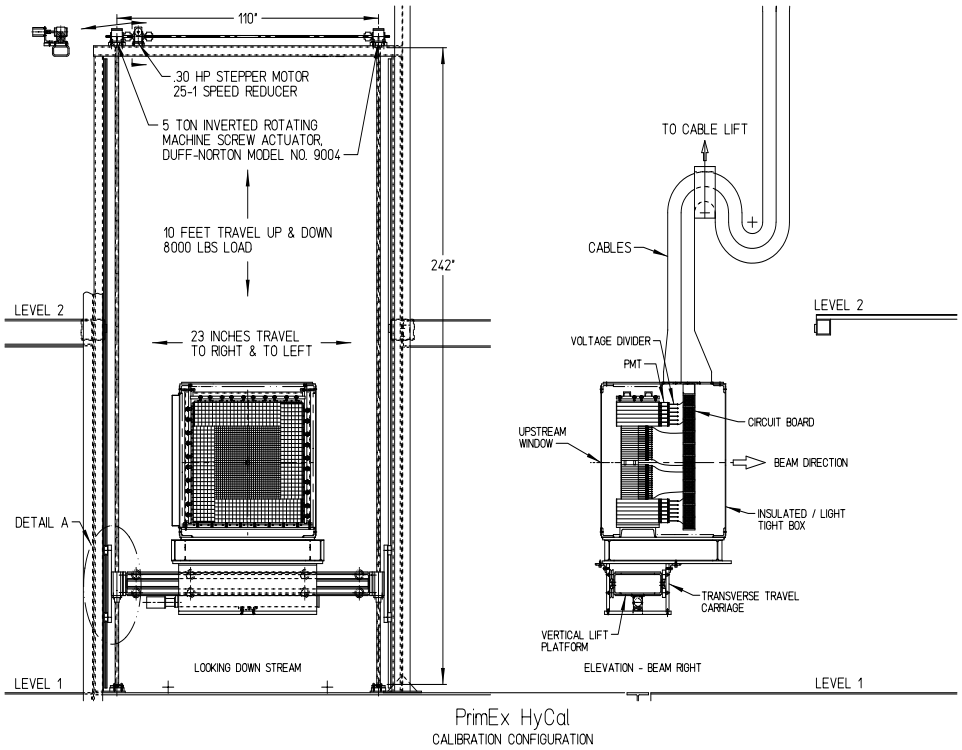

Figure 17: The HYCAL mounted on its transporter.

using the "LMS events". The results of the initial calibration (at 1200 V) and corrected one (at 1170 V) are presented in the top picture of the figure 19. The correction factor is on the order of 0.6 at 1170 V comparing to 1200 V, which is about a 40% reduction of the initial signal. The correction accuracy is plotted in the bottom picture. Error bars include statistical and systematic errors (including errors due to fitting procedure).

3.9 Veto Scintillators

The veto counters are an array of scintillator paddles in front of the calorimeter that serve to veto charged particle backgrounds. Ten scintillators with PMT readout on both ends will cover the full solid angle spanned by the calorimeter. In order to minimize photon conversion, only a single 1/4" thick layer of scintillator will be used. Time differences between signals from the two ends of the scintillator will be used to determine the position of the incident particles.

In the PrimEx Jeopardy Proposal, the collaboration had decided to investigate the possibility of using some currently existing veto counters from the UVA G_n^E experiment. However, the UVa paddles are 40 cm longer than required by *PrimEx* and light loss in the scintillator is a major concern. After testing the paddles at the University of Massachusetts Amherst, the collaboration decided to build its own set of veto counters which are the length *PrimEx* requires.

Currently, a majority of the veto counters have been built and tested. Out of the 13 veto counters (12 for use, one spare) that we have parts for, eleven are built. They

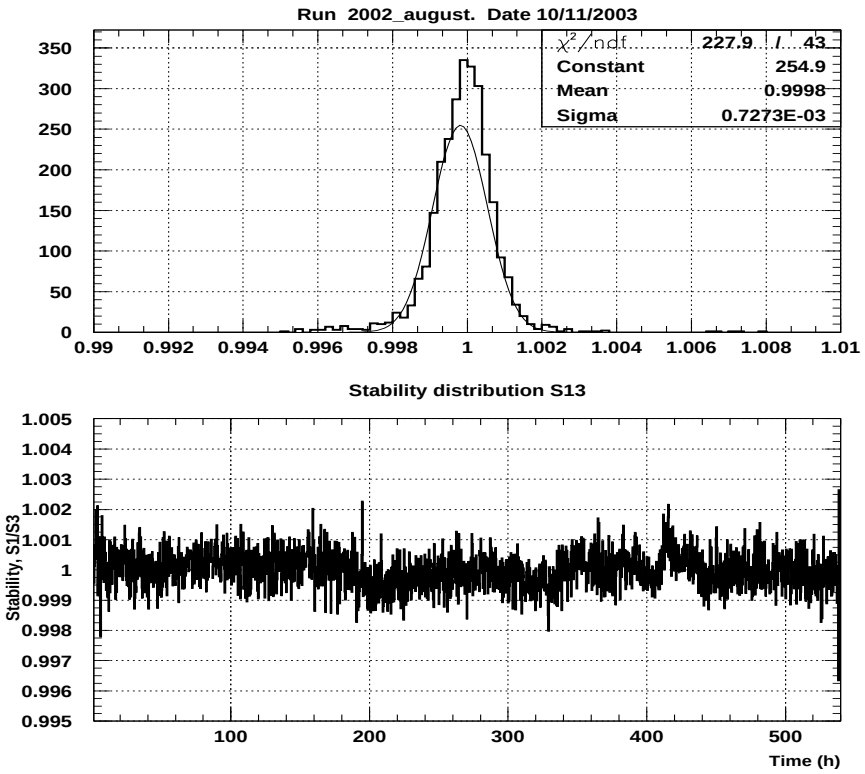

Figure 18: Stability of the light monitoring system: August 2002.

have been successfully bench tested using an oscilloscope with cosmic rays. The remaining two unfinished veto counters are waiting for a final recommendation from the University of Massachusetts Amherst collaborators and collaboration approval regarding the central beam hole size. Since rate will be high at beam center, the HYCAL does not have lead tungstate crystal detectors in this region. As such, the coverage of the veto counters will have a corresponding hole in the center of the detector. Monte Carlo work regarding the question of the beam hole cut-out is done and the results merely await presentation to the *PrimEx* collaboration.

4 Luminosity

4.1 The Tagged Photon System

The primary advantages of the *PrimEx* experiment over the previous Primakoff experiments arise from the possibility of using the Jefferson Lab Hall B tagging facility to carefully control systematic errors and reduce backgrounds. First, the tagging technique will enable a significantly more accurate knowledge of the photon flux. Second, it provides a good knowledge of the absolute photon beam energy.

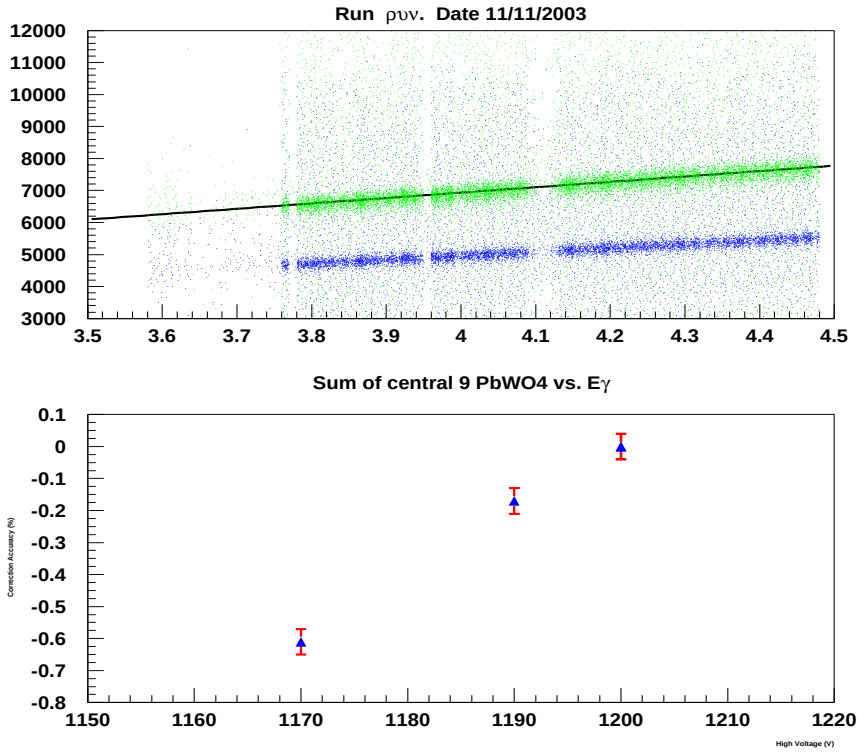

Figure 19: HYCAL-0 Beam Calibration, August 2002. Top is calibration plot. Bottom is the correction accuracy plot in per cent.

We will use a 6 GeV electron beam incident on a thin (10^{-4} radiation length) bremsstrahlung converter foil. The post-bremsstrahlung electrons will be momentum analyzed in the Hall B photon tagger magnet and photons will be tagged in the energy range from 4.6 to 5.7 GeV. The Hall B bremsstrahlung photon tagging system spans the photon energy range of 20% to 95% of the incident electron energy. The detector system consists of two planes of counters: 384 overlapping scintillators which define 767 fine energy channels of width 0.001 E_e (the "E" counters), and 61 larger scintillators, each read out by two photomultiplier tubes and designed for good time resolution (the "T" counters). The sizes of the T-counters are designed to produce approximately equal counting rates in two groups. When all 61 T-counters are used, the total tagging rate can be as high as 50 MHz for the whole focal plane. Counters T1-T19, which span the photon energy range from 77% to 95% of E_e, are proportionally smaller than the others, and will allow a tagging rate of up to 50 MHz in this region alone. This experiment will use only the "high-rate" counters T1-T19. The tagger trigger signal will be formed by taking the coincidence of the left and right PMT's of the T-counters, while the tagger Master OR (MOR) will be produced by ORing the T-counter coincidence channels.

Upgrades to the tagger E counters have been performed. New E counter electronics were fabricated in Italy and have been installed in Hall B. Testing is currently underway.

These electronics will greatly improve instability problems in the E counters, as well as provide greatly improved flexibility in that thresholds, delays, and gate widths will be fully programmable. This software has been developed by the Glasgow group.

4.2 Absolute calibration with total absorption counter

Since each π^o decay event is measured in coincidence with a tagging counter signal, the normalization of the cross section to the incident photon flux depends on knowing the number of tagged photons on target in each energy bin during the run. The number of tagged photons on target is not necessarily equal to the number of events recorded by the tagging counters because of a number of effects:

(1) events in which a bremsstrahlung photon is produced but is absorbed before reaching the target.

(2) Møller scattering events in the bremsstrahlung radiator which produce an electron in the tagging counters without an accompanying photon.

(3) Extra post bremsstrahlung electrons registered due to room background.

Events of the first type will be minimized by allowing the entire bremsstrahlung beam to travel in vacuum without collimation to the target. The second category of events is known to affect the tagging rate at the level of a few percent. The combination of these first two effects can be measured by performing a calibration run in which the Primakoff target is removed and a lead glass total absorption counter (TAC) is placed in the photon beam. The ratio of Tagger·TAC coincidences to tagger events, the so called tagging ratio, is then recorded.

Knowing this ratio, one can determine the tagged photon flux in the data taking run by counting the number of post bremsstrahlung electrons in a given tagging counter:

$$N_\gamma^{tagged}(experiment) = N_e(experiment) \times \frac{N_\gamma^{tagged}(calibration)}{N_e(calibration)} \tag{1}$$

One can then determine the cross section from the tagged yield of π^o's:

$$\text{TaggedYield} = \frac{d\sigma}{d\Omega} \times t \times \Delta\Omega \times \epsilon_{\pi^o} \times N_e(experiment) \times \frac{N_\gamma^{tagged}(calibration)}{N_e(calibration)}, \tag{2}$$

where t is the target thickness, $\Delta\Omega$ is the solid angle of the pion detector, and ϵ_{π^o} is its two photon efficiency. In the calibration run, the total absorption counter rate is limited, and therefore the tagging efficiency must be measured at a rate which is reduced by a factor of about one hundred as compared to the data taking run. As such, any rate dependence in the tagging efficiency must be considered.

4.2.1 Total absorption counter status

A new total absorption counter (TAC) has been built by the *PrimEx* Collaboration which consists of a single $20 \times 20 \times 20 \times 40 cm^3$ lead glass block (SF5, $L = 17X_o$). It has a single 5" Hamamatsu PMT (R1250, rise time $\sim 2.5ns$) attached to it and is instrumented with both an ADC and TDC. In the August 2002 test run, with a 100 pA electron beam and a $2 \times 10^{-5} X_o$ bremsstrahlung radiator, the TAC fired at about 100kHz with a 35 mV threshold.

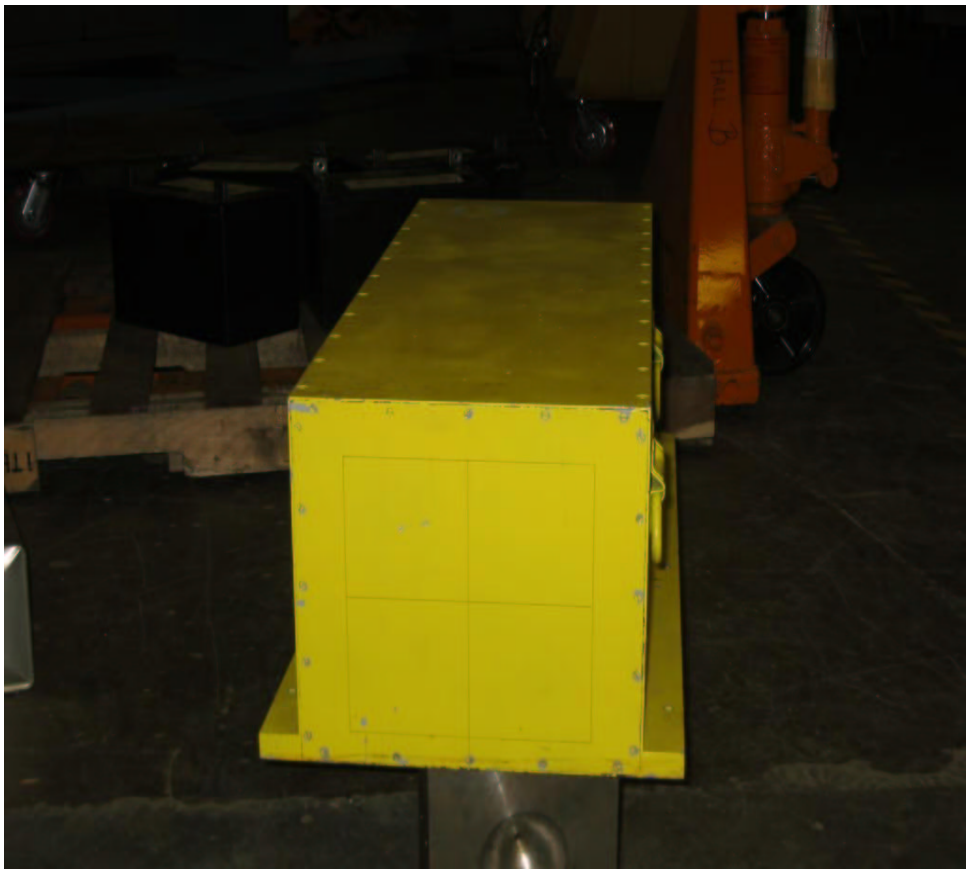

Figure 20: The Total Absorption counter (TAC).

The absolute normalization of the experiment hinges upon the assumption that the TAC has 100% efficiency for detecting photons in the tagging energy range. As such, studies of the tagging ratios as a function of TAC threshold are planned. In August 2002, the TAC underwent initial commissioning. Figure 21 shows the measured tagging ratios across the tagged photon energy range from 0.77 to $0.95\%E_o$. Given that there was a $5\%X_o$ target in place, the tagging ratios are close to what one would expect. Further studies without a target and with varying tagging rates are planned.

4.3 Relative calibration with pair spectrometer

The use of the total absorption counter to calibrate the number of photons per tagging electron will provide an absolute calibration of the photon flux incident on the π^o production

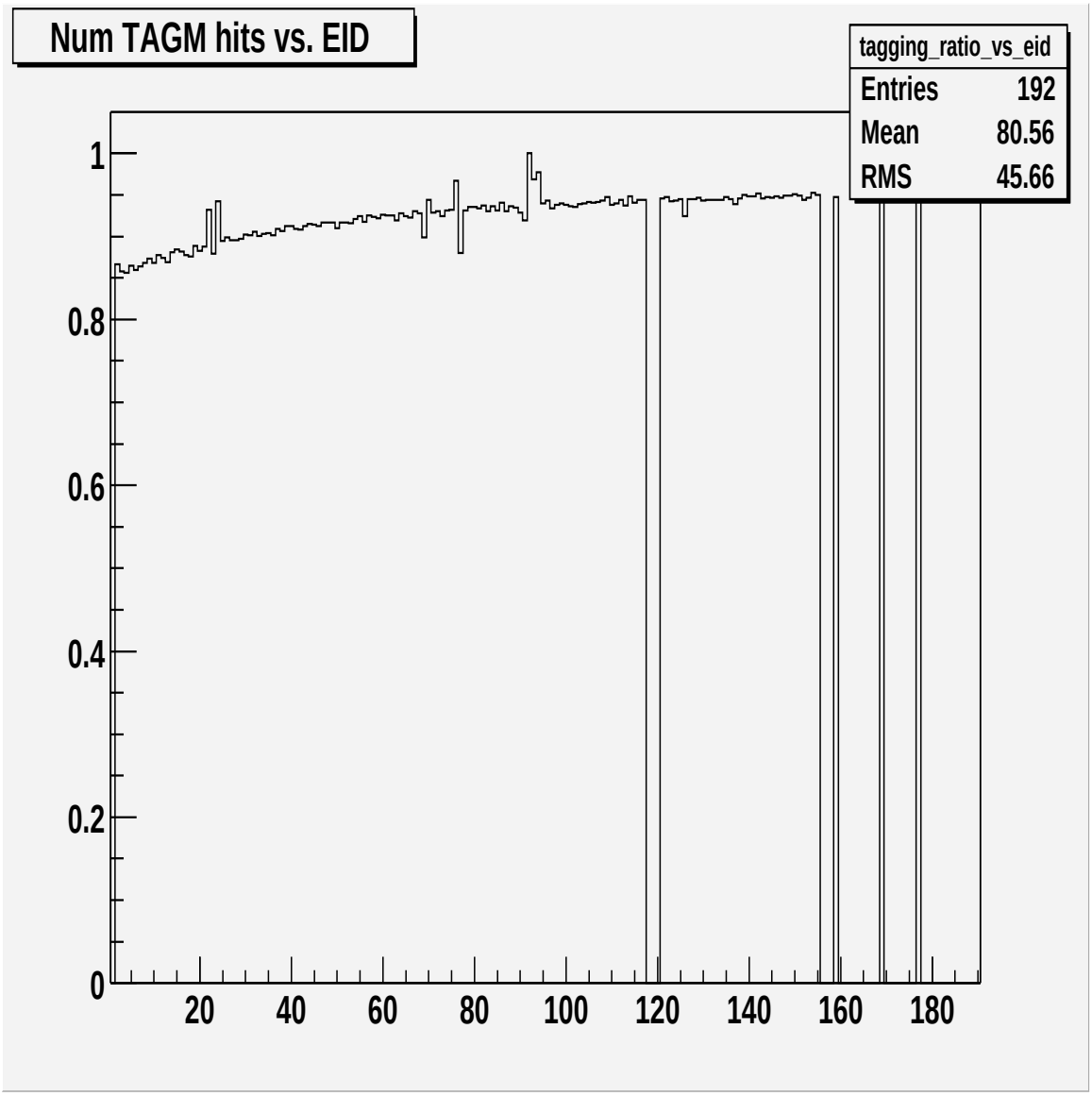

Figure 21: Tagging ratio as measured with the PrimEx TAC in August 2002 test run. A $5\%X_o$ target is placed at the PrimEx target postion between the bremsstrahlung radiator and the TAC.

target. However, these measurements will be performed at intervals throughout the data taking, and will by necessity be performed at an electron beam current which is two orders of magnitude less than the production data taking runs. Consequently, we have constructed a pair production luminosity monitor which will measure the relative tagged photon flux over a range of intensities, and will operate continuously throughout the data taking runs.

The pair spectrometer will use the physics target as a converter, and will make use of the 15 kgauss-meter dipole magnet placed just downstream of it. The electrons and positrons are detected on either side of the beam in a series of plastic scintillator telescopes. The requirements of the pair spectrometer are that it must operate over the entire range of intensities (of both the flux calibration and data taking runs) and have a smooth, relatively flat acceptance in E_γ covering the entire tagging range. The segmentation of the pair spectrometer detectors is driven by the fact that the pair production and Primakoff target are the same, and therefore the pair spectrometer detectors must accommodate the rates from a 5% radiation length target. Under the *PrimEx* run conditions, we expect singles rates on a single telescope to be about 140kHz, and a total of 90kHz of pair spectrometer-tagger coincidences over the range of tagging energies from $0.77E_o$ to $0.95E_o$. The efficiency of the pair spectrometer for tagging photons will be about 0.6%. A schematic of the pair spectrometer with one simulated pair production event is shown in figure 22, and a photograph of the device is shown in figure 23. Each arm presently consists of eight telescopes with overlapping momentum acceptances placed symmetrically on either side of the beamline. We are currently in the process of upgrading this to 16 telescopes on each side (for a total of 64 detectors) to provide the ability to tag photons over nearly the entire range of the Hall B tagger, from $0.2E_o$ to $0.95E_o$.

4.4 Results from August 2002 Test Run

In August 2002, we performed a series of beam tests to ascertain whether the relative tagging efficiencies, as measured by the pair spectrometer, were independent of the beam current at the one percent level. For TAC calibration runs, we measure the absolute tagging ratio:

$$R_{absolute} = \frac{N^{TAC}_{\gamma \cdot e_i}}{N_{e_i}} \tag{3}$$

where $N^{TAC}_{\gamma \cdot e_i}$ is the number of photons, as measured in the TAC, in coincidence with tagging counter i, and N_{e_i} is the number of electrons in tagging counter i. With the pair spectrometer, we can measure the relative tagging ratio:

$$R_{relative} = \frac{N^{ps}_{e^+e^- \cdot e_i}}{N_{e_i}} \tag{4}$$

where $\frac{N^{ps}_{e^+e^- \cdot e_i}}{N_{e_i}}$ is the number of pair production events in coincidence with a given tagging counter. While this is a relative number, its normalization can be fixed with the TAC, and it has the advantage of the possibility of measurement over all relevant currents, *i.e.* the high currents of the production data taking and the low currents at which the absolute tagging ratios are measured with the TAC. In August 2002, we measured $R_{relative}$ from 10 to 100 nAmps, and the results are shown for one T counter (T9) in figure 24. As can be seen,

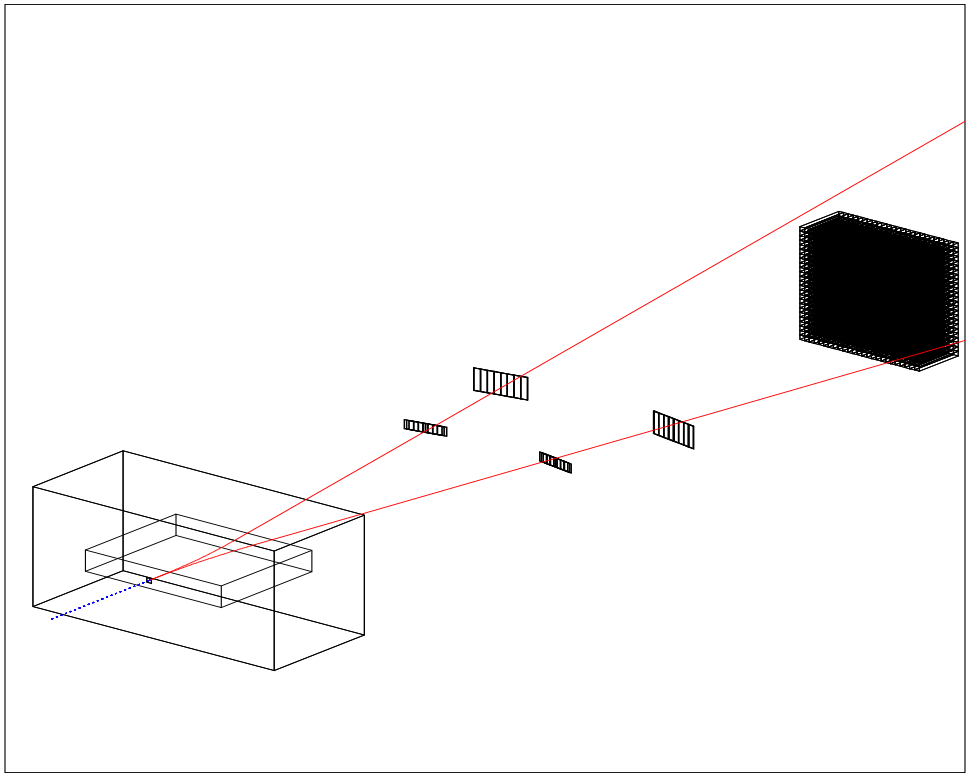

Figure 22: Layout of the luminosity monitor and one pair production event. Each detector arm is currently segmented into eight contiguous plastic scintillator telescopes.

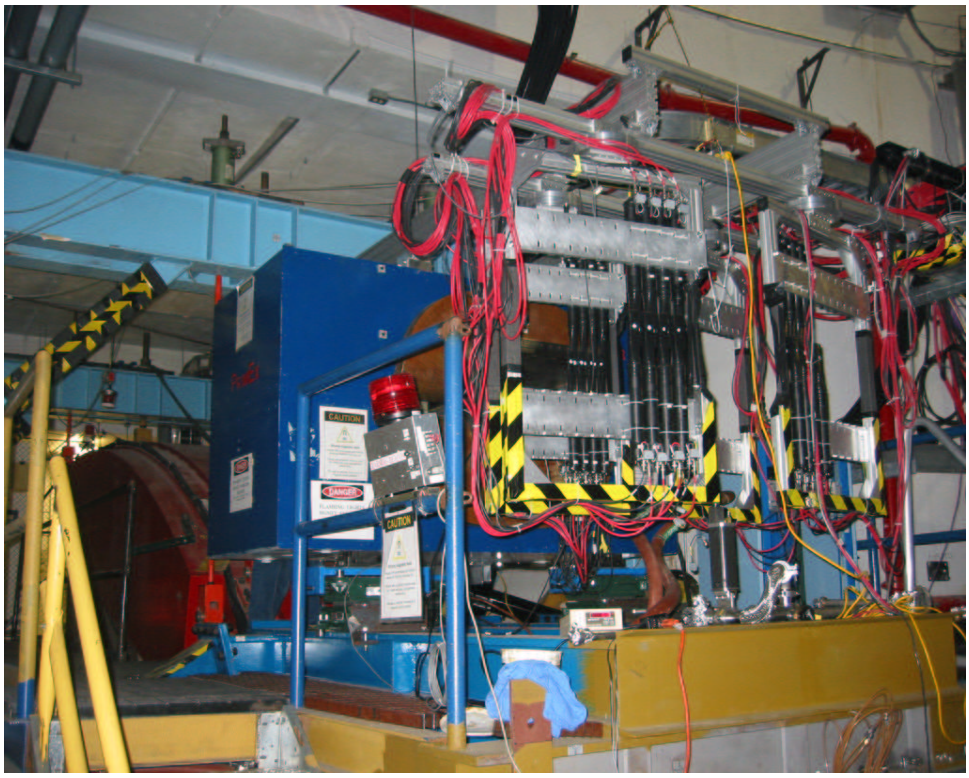

Figure 23: The *PrimEx* pair spectrometer.

$R_{relative}$ is quite independent of the beam current. In these and all subsequent plots, only the T counters were taken into consideration (no E-T coincidences), and accidentals between the pair spectrometer and the tagger were subtracted.

Figure 25 shows the relative tagging ratios across the tagger focal plane for two photon fluxes differing by a factor of ten. The energy dependence of $R_{relative}$ arises from that of the pair production cross section as well as the energy acceptance of the pair spectrometer as determined by the acceptances of the pair spectrometer detectors and the pair spectrometer magnetic field setting. A GEANT simulation of the efficiency of the pair spectrometer to tag a photon of a given energy (under the conditions of the August 2002 run) is shown in figure 26 where it can be seen that the magnitude of the efficiency of the pair spectrometer to tag a photon is roughly as expected ($\sim 0.6\%$).

To combine information from all 20 T counters, we have proceeded as follows. For a given T counter, we have calculated the average relative tagging efficiency, where the average is over the four different currents of the run. Then, for each beam current and each T counter, we have calculated the deviation from the average for each T counter. As shown in figure 27 this gives:

$$\frac{\delta R_{relative}}{R_{relative}} = 1.02\%, \tag{5}$$

which is at the 1% level required by the experiment. Similar measurements at lower currents are planned in our upcoming luminosity test run.

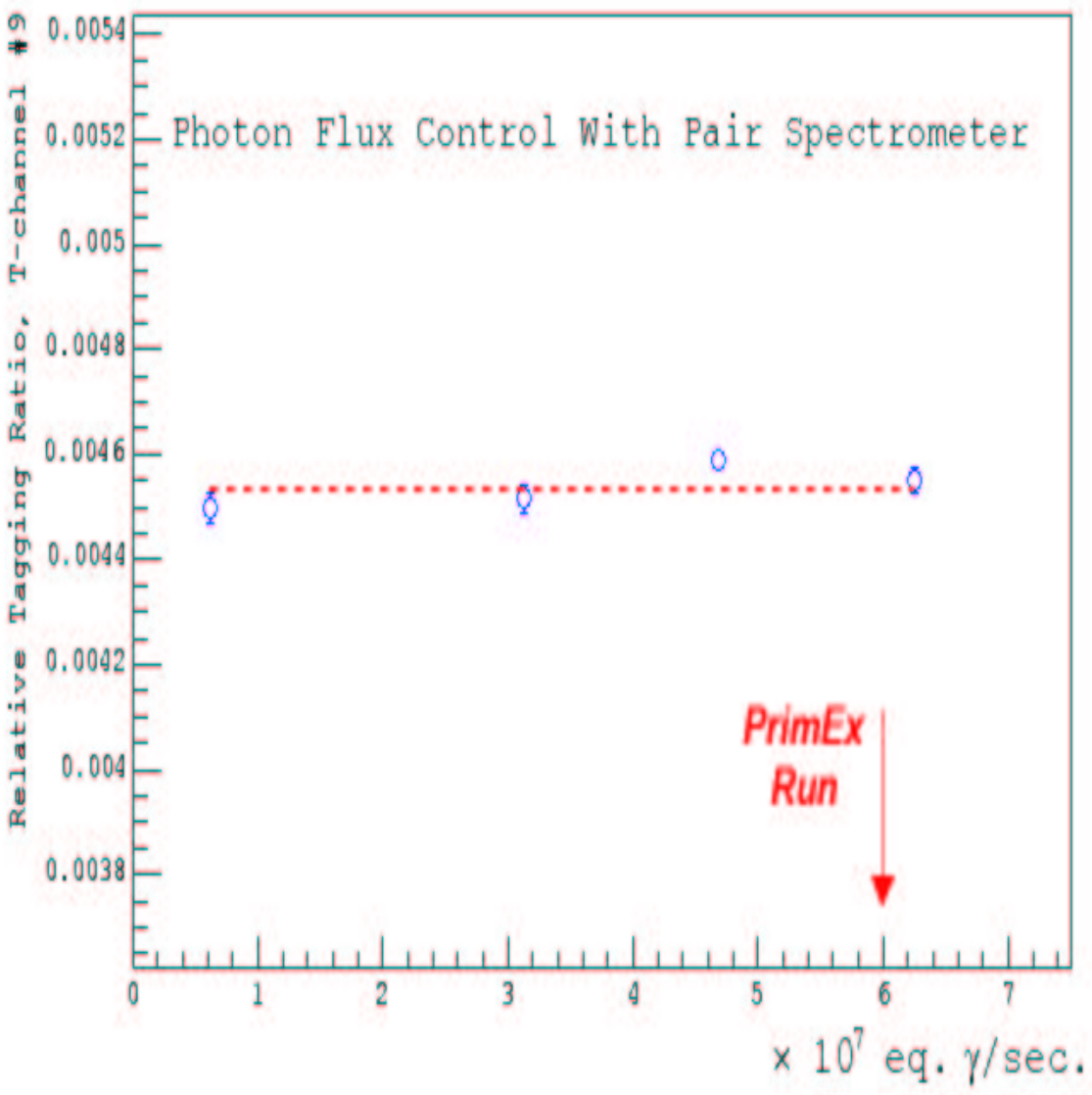

Figure 24: Measured relative tagging ratios for T counter 9 as a function of photon flux.

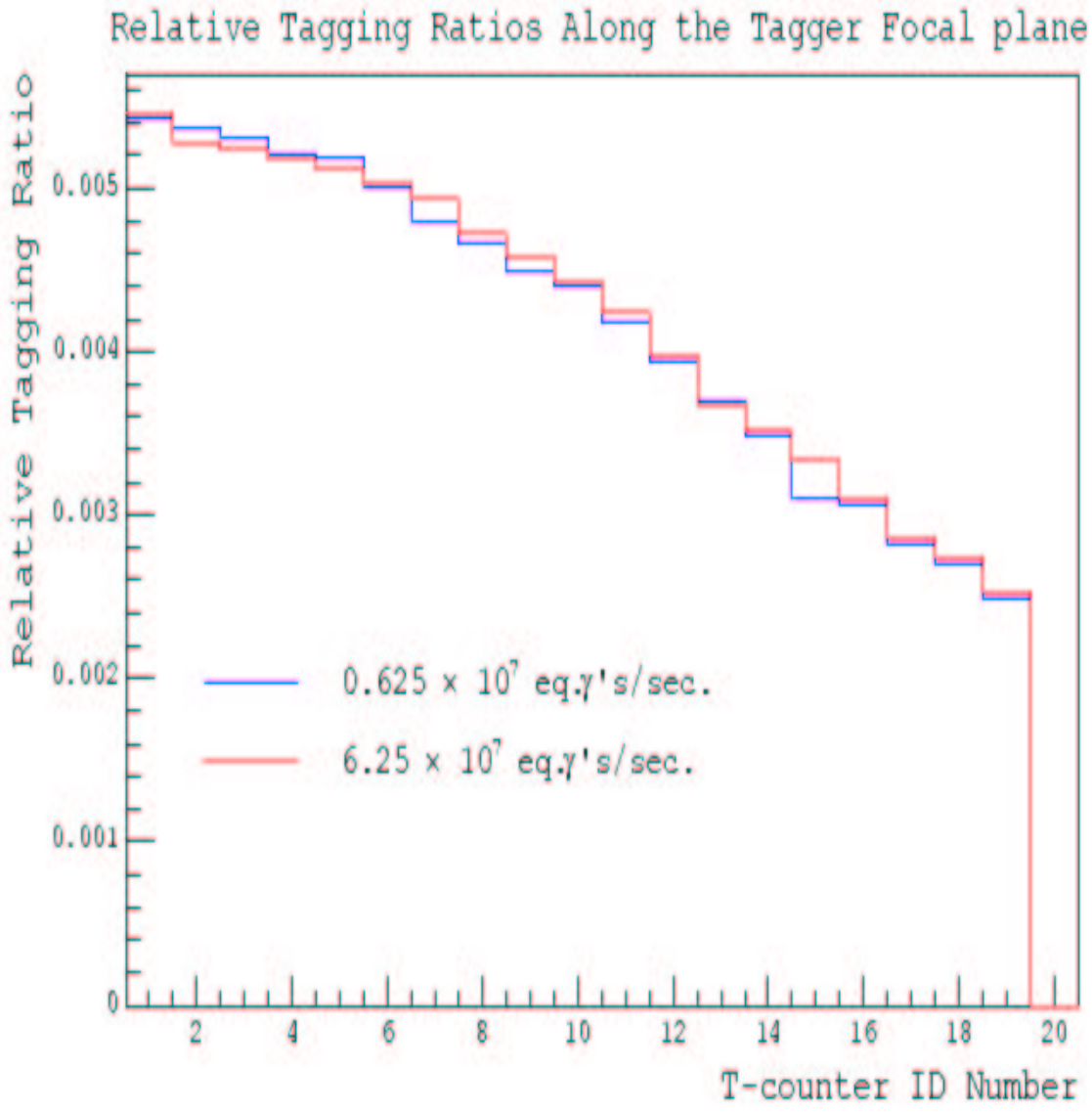

Figure 25: Relative tagging ratios as measured by the *PrimEx* pair spectrometer for each of the 19 T counters and for two different photon fluxes..

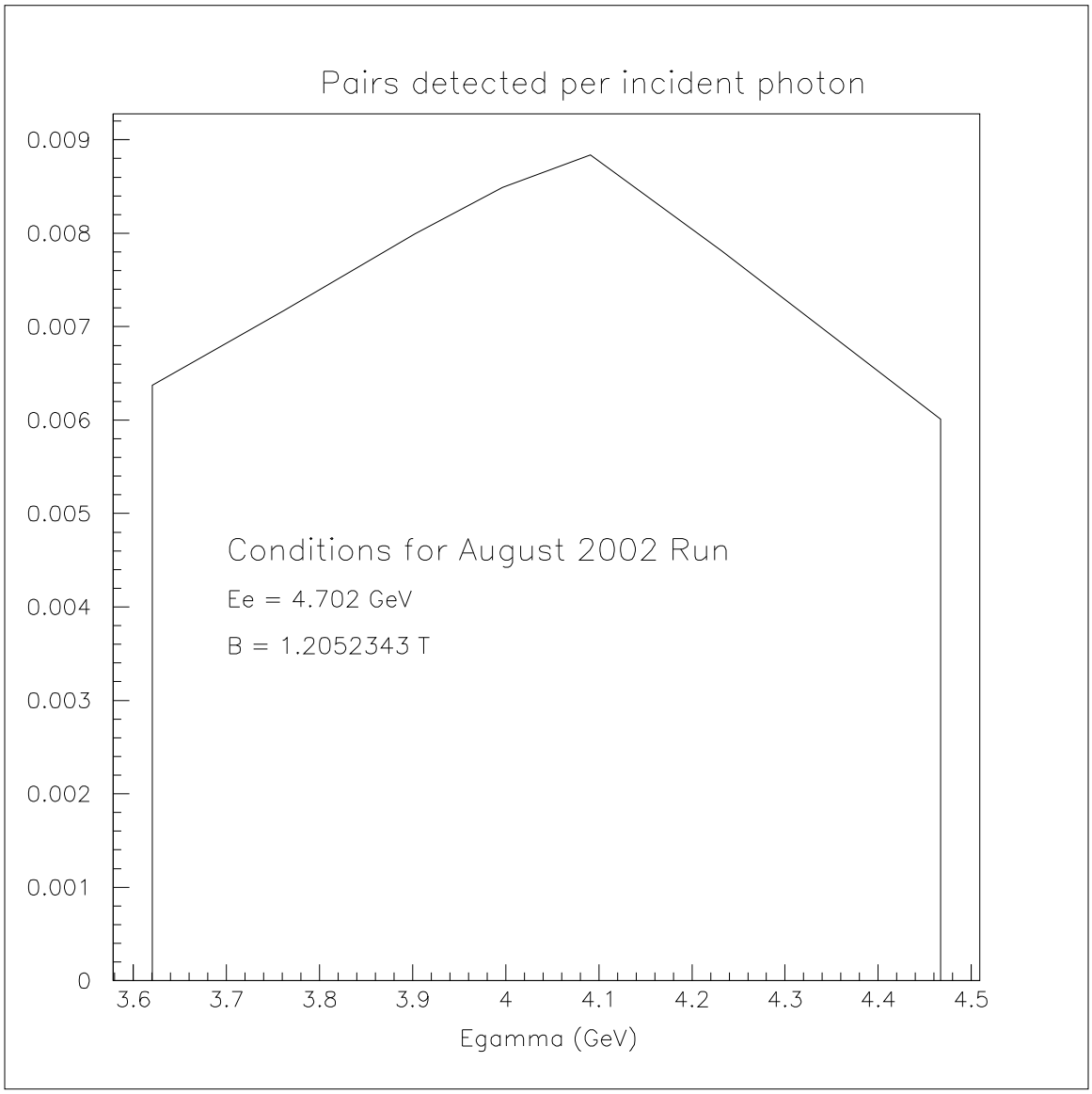

Figure 26: Calculated efficiency for the pair spectrometer to tag a photon of a given energy under the conditions of the August 2002 run.

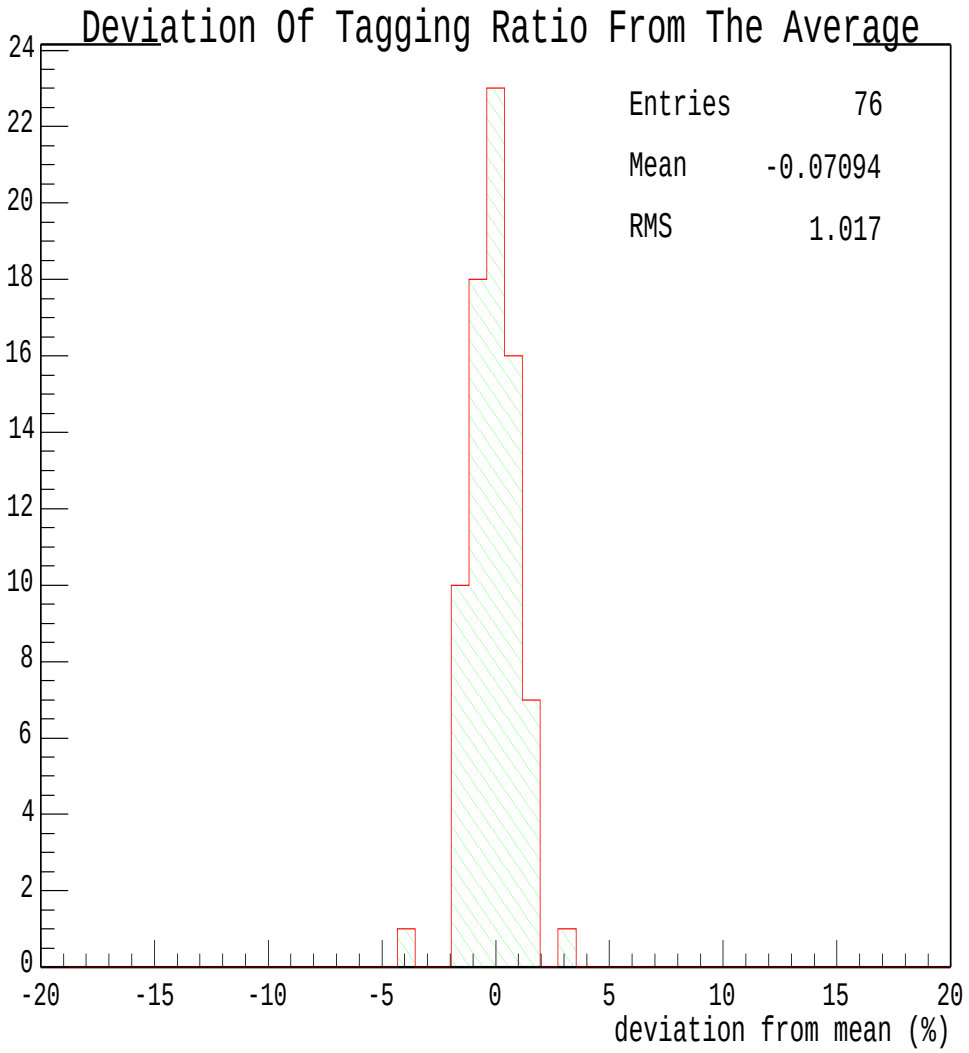

Figure 27: The difference in relative tagging ratio for each T counter from the mean for each of the four different runs done at different beam currents (19 T counters $\times$ 4 runs = 76 entries.)

This analysis was done using a MOR trigger. That is, the $PS \cdot T_i$ coincidences were determined from the associated TDC spectra, and the number of electrons for a given tagging counter were determined by the coincidence in the TDC spectrum of T_i with the MOR.

4.5 Electron counting by sampling method

As stated previously, the number of tagged photons on target during the production data taking is given by:

$$N_\gamma^{tagged}(experiment) = N_e(experiment) \times \frac{N_\gamma^{tagged}(calibration)}{N_e(calibration)} \tag{6}$$

The steps we have taken utilizing the pair spectrometer to ensure $\frac{N_\gamma^{tagged}(calibration)}{N_e(calibration)}$ is rate independent have been described. While this ratio is measured using a Master Or (MOR) trigger, data acquisition rate considerations require that the primary trigger during the production data taking runs be of much lower rate than the MOR. $N_e(experiment)$ could be determined via a sampling technique which involves counting electrons which are out of time with a HYCAL trigger. Individual tagging counters are each fed into a multi-hit TDC (LRS1877). Two important features of this module are its deadtime (25 ns self inhibit deadtime) and its LIFO (Last In First Out) limit. The LRS1877 TDC module has a programmable LIFO up to 16 hits per event per channel. Out of time electrons will be integrated over a range which excludes the triggering events and any depletion due to LIFO limits. Figure 28 shows such a time distribution, with the shaded area representing the range that would be used. The integral is divided by the product of the integration interval and the number of events over which the distribution was accumulated. Deviation from a perfectly flat distribution over this range would be indicative of a problem.

Sensitivities of this method to beam current fluctuations can be minimized by requiring the electron sampling be governed by a trigger which, unlike the HYCAL trigger, is independent of the beam current. As such, we will implement a clock trigger for electron counting purposes. This will greatly minimize the impact of LIFO corrections.

For the technique described above, a typical tagging counter will run at about 1MHz. An alternative technique involving the use of the pair spectrometer can be simultaneously employed which will greatly minimize the effects of LIFO and deadtime.

As discussed previously, the absolute tagging ratio is determined in a low flux calibration run using the total absorption counter and a Master Or (MOR) trigger:

$$R_{TAC} = \frac{N_{\gamma \cdot e}(calibration)}{N_e(calibration)} \tag{7}$$

Similarly, one can measure the relative tagging ratio with the pair spectrometer. In this case one can also use a MOR trigger and, for reasons which will be clear shortly, it is to be measured at high rates.

$$R_{PS} = \frac{N_{e^+e^- \cdot e}(\text{calibration, highrate})}{N_e(\text{calibration, highrate})} \tag{8}$$

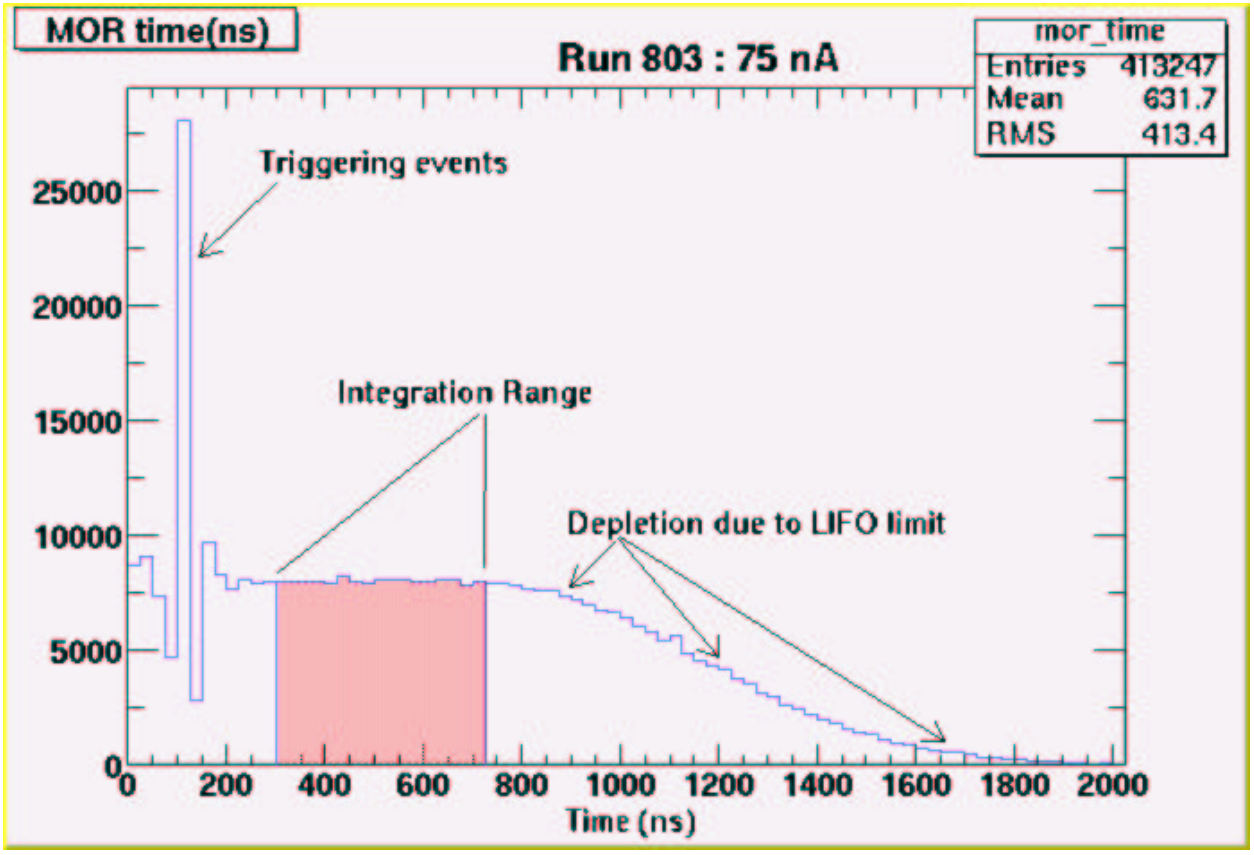

Figure 28: MOR (hardware OR of top 19 Tagger T-counters) time distribution. The shaded area represents the range of integration.

If one measures the number of $e^+ - e^-$ pairs in coincidence with a given tagging counter during the data taking run, the total tagged photon flux is then given by:

$$N_\gamma^{tagged} = \frac{R_{TAC}}{R_{PS}} N_{e^+e^-\cdot e}^{sampled}(\text{datarun}) \tag{9}$$

where $N_{e^+e^-\cdot e}^{sampled}(datarun)$ is determined by sampling in a manner similar to that described above. The advantage of this approach is that the pair spectrometer rate is an order of magnitude lower than that of a typical T counter and thus deadtime effects are considerably less. Both techniques will be employed in the *PrimEx* run.

4.6 Target thickness measurements

Three experimental targets will be employed in the *PrimEx* experiment – ^{12}C, ^{120}Sn, and ^{208}Pb – each 5% of a radiation length in thickness. In the Primakoff process the reaction mechanism is simplified if the target nucleus has $J^\pi = 0^+$. Therefore, isotopically enriched materials are required for the tin and lead targets. The ^{120}Sn and ^{208}Pb targets were ordered from Oak Ridge National Laboratory at a cost of approximately \$12.5k and delivered in early summer of 2001. The enrichments are 98.29% for the tin target, and 99.09% for the lead target.

In this experiment, we require that the target thickness, ρ_t, be known to a precision better than $\pm 0.7\%$. In principle this tolerance can be satisfied by micrometer measurements with an accuracy of ± 0.05 mil, and micrometers of this accuracy are commercially available. However, use of a micrometer could produce indentations or bends in the metal foils. For this reason we have performed direct measurements of the metal foils with a technique that avoids direct contact with the target. X-ray attenuation represents the basis for such a determination. In this technique a line source of X-rays is collimated to a spot size a few mm in diameter and detected in a NaI detector behind the target foil. For these measurements we use the 60 keV X-ray line from ^{241}Am. The attenuated X-ray intensity through the foil is given by:

$$I(T) = I_0 B(T) e^{-T/\lambda}$$

where I_0 is the unattenuated intensity, T is the target thickness, λ is the X-ray attenuation length, and B(T) is the buildup factor. Provided that λ and the functional dependence of the buildup factor on T are known, T can be obtained from a measurement of the attenuated X-ray flux through the target foil.

Purely exponential attenuation, where the buildup factor B(T) is unity, is only realized in a situation where the X-ray collimation is perfect and the X-ray detector subtends zero solid angle. In more realistic situations, Compton scattering in the target foil leads to non-exponential attenuation. Using 60 keV X-rays and tin and lead foils of approximately 5% radiation lengths in thickness, we found that the buildup factor can be empirically parameterized by

$$B(T) = 1 + bT/\lambda$$

where b is a constant, approximately 0.07 for tin, and 0.15 for lead. Therefore, the flux decreases more slowly with increasing foil thickness than for pure exponential behavior. We found no evidence that higher order terms in T/λ play a significant role in the buildup factor for 5% radiation length targets.

To calibrate the measurements, we first make a micrometer measurement at one point on the target and then X-ray that point. This provides a calibration for the parameter b. The X-ray attenuation lengths are known with sufficient accuracy at 60 keV for tin and lead, at about the 1% level, and can be taken from the literature. Then other points of the target are X-rayed and the target thickness obtained from the attenuated X-ray flux. We will take a micrometer measurement on at least one other point of the target to cross calibrate the procedure.

The targets will be scanned over the X-ray source to obtain a map of ρ_t as a function of x and y. Scanning a thick high-Z wire through the beam fiducializes the position of the X-ray beam. In this case we look for a dip in the count rate as the wire passes through the X-ray beam.

The X-ray scan apparatus has been designed and constructed and is controlled by LabView. A 1" NaI crystal is used to the detect X-rays and the NaI pulse height is readout through a CAMAC ADC system, also running under LabView control.

The carbon target is machined from a block of pyrolytic graphite (PG) of natural isotopic purity. PG is a crystalline form of graphite that is produced using high temperature Chemical Vapor Deposition furnace technology. The low porosity of PG, approximately 1%, as compared to 10% for normal graphite makes it an ideal material for use as a target. The PG density depends somewhat on the specifics of the manufacturing process. However, PG densities are typically close to the theoretical limit of 2.25 g/cm^3. We will measure the density of the PG target in a specific gravity setup using an electronic scale and ultrapure water. Laboratory tests have indicated that we can achieve the required level of precision for the density. The thickness of the target (approximately 1 cm) will be measured with a micrometer; a prototype target machined from a block of normal graphite had thickness variations of approximately 0.1%. Finally, as a last check on ρ_t, we will X-ray the carbon target to make sure there are no internal voids in the PG material. We have obtained a sample of PG from SLAC that is sufficiently large that several targets can be cut from it. A target has been successfully machined from the sample.

The *PrimEx* target ladder and moving mechanism have been designed, constructed and assembled by the JLab technical staff. The target ladder can move in both the horizontal and vertical directions, giving us fine control over exactly where we place the photon spot on the target. There are positions on the target ladder for six targets – the three production targets, a blank, a crossed wire to fiducialize the position of the photon beam by use of pair production, and a thin foil to be used in tests of the pair spectrometer.

4.7 Normalizing Primakoff yield to Compton yield

An alternative technique for determining the absolute Primakoff cross section can be employed which is largely insensitive to the degree in which we can determine the absolute target thickness and absolute tagged photon flux. While the previously described techniques of determining absolute target thickness and photon flux will be our primary methods, with-

out additional equipment or beamtime one may measure the Primakoff π^o yield relative to the Compton yield. This could greatly reduce the major sources of error in the experiment – photon flux, (1% error) and target thickness, (0.7% error).

The Primakoff cross section is given by:

$$\frac{d^3\sigma_P}{d\Omega} = \Gamma_{\gamma\gamma}\frac{8\alpha Z^2}{m^3}\frac{\beta^3 E^4}{Q^4}|F_{e.m.}(Q)|^2\sin^2\theta_\pi, \tag{10}$$

and the experimental Primakoff yield can then be expressed as:

$$Y_{\pi^o} = t_{target} \times \Phi_\gamma \times \Gamma_{\gamma\gamma} \times Z^2 \times \sigma_p, \tag{11}$$

where σ_p represents known constants and kinematical factors which are integrated over the (two photon) acceptance of the HYCAL detector, t_{target} is the target thickness, and Φ_γ is the tagged photon flux.

This Primakoff yield can be measured with respect to the yield of Compton scattered photons (off of atomic electrons in the target). The idea behind using electron Compton scattering comes from the fact that it is a calculable, pure QED process. Ignoring the radiative corrections for simplicity, the cross section is given by the Klein-Nishina formula:

$$\frac{d\sigma}{d\Omega} = Zr_o^2\frac{1+cos^2\theta}{2}\frac{1}{1+\gamma(1-cos\theta)^2}[1+\frac{\gamma^2(1-cos\theta)^2}{(1+cos^2\theta)(1+\gamma(1-cos\theta))}] \tag{12}$$

Or, one could write:

$$Y_{Compton} = t_{target} \times \Phi_\gamma \times Z \times \sigma_{Compton}, \tag{13}$$

Taking the obvious ratio, we get:

$$\frac{Y_{\pi^o}}{Y_{Compton}} = Z \times \Gamma_{\gamma\gamma} \times \frac{\sigma_P}{\sigma_{Compton}}, \tag{14}$$

independent of the target thickness and tagged photon flux.

Figure 29 shows the energy-angle correlation of scattered photons incident on HYCAL as generated by GEANT, with kinematical cuts on the Compton process as shown. The primary electromagnetic background comes from pair production followed by bremsstrahlung. Photon singles rates due to hadronic production will also be an issue. In the PrimEx proposal presented at PAC15, total singles rates from ω production were estimated to be less than 1 Hz (figure 26c of the proposal), with those from ρ production estimated to be about ten times those of the ω. This compares favorably with the 500 Hz Compton rate.

Since the cross section for Primakoff production increases with energy, and the cross section for Compton scattering decreases with energy in this energy range, the ratio will be more sensitive to the energy calibration than Primakoff production alone. A 1% error in incident photon energy gives a 1% error in the π^o radiative width. Thus, the effectiveness of this technique is directly tied to the energy calibration.

The acceptance of Compton events is also more sensitive to the size of the central hole in the fiducial volume of HYCAL than the Primakoff acceptance. A $1mm$ error gives a 0.5% error in the Compton yield. While there is some cancellation of this error in taking the Compton to Primakoff ratio, this cancellation is quite small.

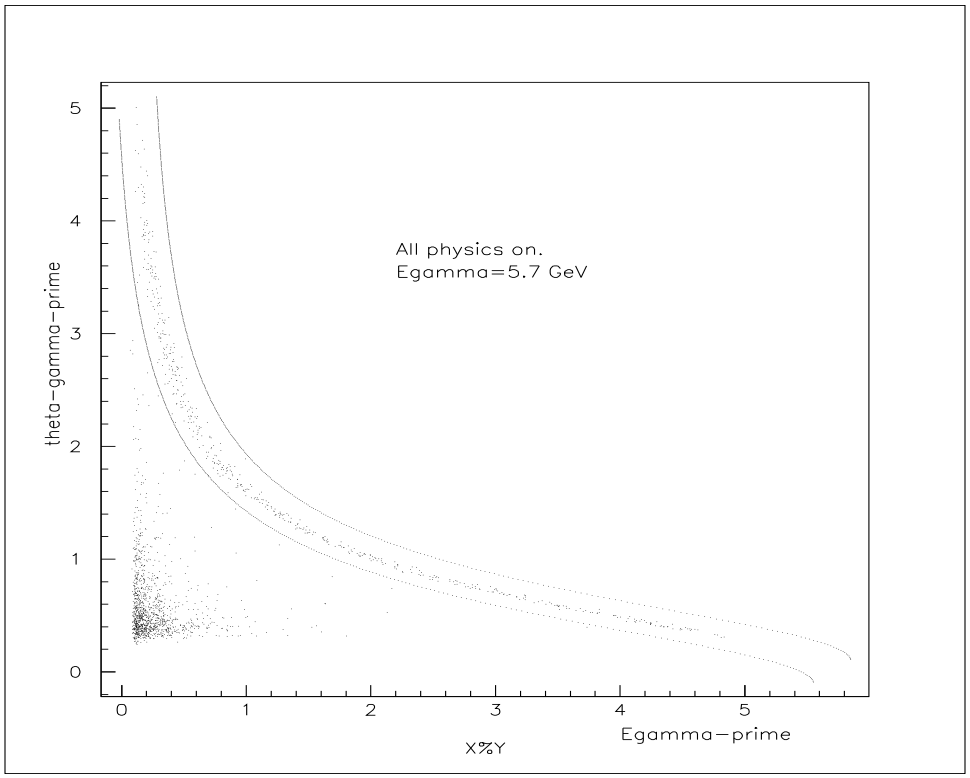

Figure 29: Kinematical correlation between Compton scattered photon energy and scattering angle as generated by GEANT. All physics processes are turned on, and the "Compton event" cuts are shown.

To summarize, this technique shows promise as an alternative to that relying on the TAC and the pair spectrometer. It requires no new major instrumentation or beam time. Its main advantage is that it essentially eliminates the need to know the target thickness and tagged photon flux.

4.8 Plans for a future luminosity beam test

The *PrimEx* Collaboration plans a two day luminosity monitoring test run before major installation and commissioning of the HYCAL. The key goals of this run will be:

I. Determine whether the relative tagging efficiency, as measured by the pair spectrometer is rate independent at the 1% level over the ranges of photon fluxes spanning those of the TAC runs to those of the production data taking runs. This includes runs with two different pair production target thicknesses.

II. Commission the TAC, and determine the absolute tagging ratios over the largest range of currents possible and ensure they are independent of rate.

III. Determine the tagging ratios as measured with the TAC with and without a $4cm \times 4cm$ collimator in front of it. This will mock up the geometry of the HYCAL and ensure that placing the TAC behind the HYCAL will not decrease the measured tagging ratios and thereby introduce systematic errors.

IV. Test clock trigger method for electron counting.

V. Commission a new online beam profile monitor.

VI. Implement ADC's for pair spectrometer detectors to study rate dependence of pulse heights.

5 Data Acquisition and Electronics

5.1 Electronics Overview

The *PrimEx* electronics will consist of Fastbus, VME, CAMAC, and NIM standards crates. The digitization will be done entirely by Fastbus LRS1877 TDC and LRS1881M ADC modules. Additionally, some VME scalers will be read out and periodically inserted into the datastream. The triggering electronics will be done using NIM modules for fanning in calorimeter signals and discrimination. Three CAMAC programmable memory lookup units will implement the logic of the trigger.

5.1.1 Crates and Modules

The various crates used to hold the *PrimEx* electronics will be fixed in four electronics racks which are of the same style as those already in use in Hall-B. A diagram illustrating the layout of these crates is shown in figure 30. A total of 30 LRS1881M ADC modules will be required. The space required for each delay cable bundle prevents any ADC modules from

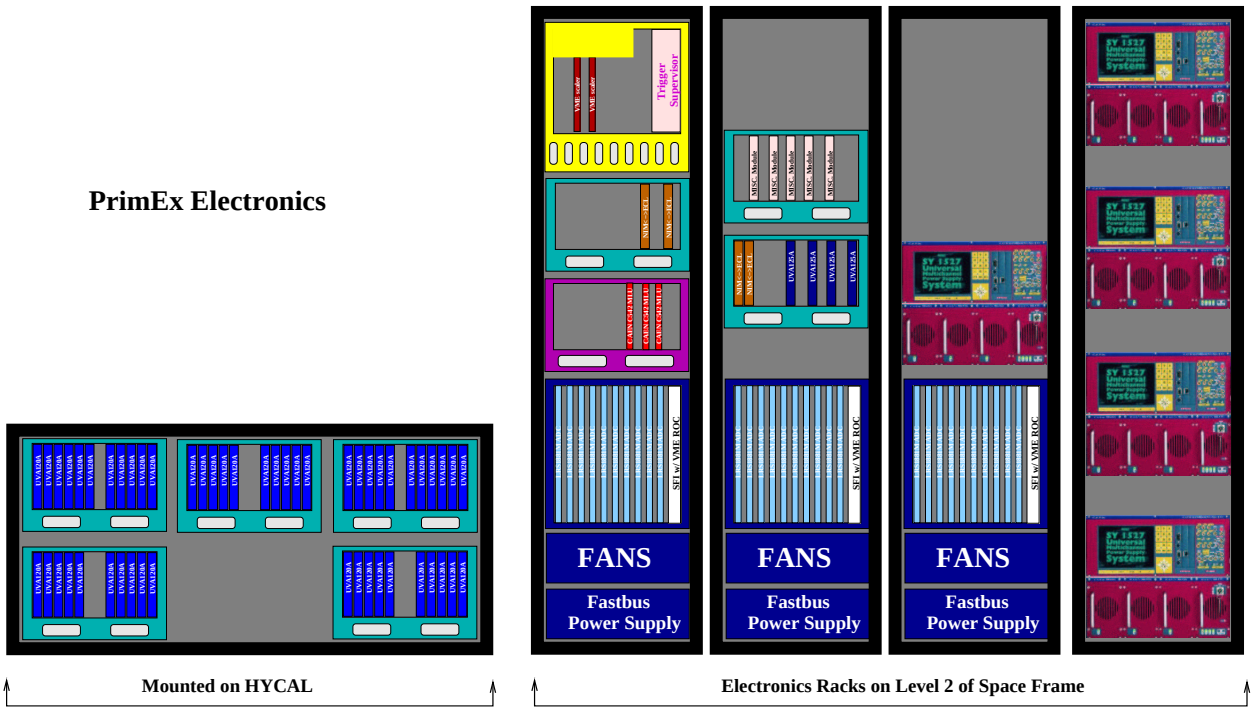

Figure 30: Map of PrimEx Electronics Racks. This is not exactly to scale, but it is reasonably close.

being placed in adjacent slots. Thus, three fastbus crates are needed to hold all 30 ADC modules and one LRS1877 TDC module.

The trigger (described in section 5.2.1) is based on UVA120A and UVA125A NIM modules. The design of these modules was modified specifically for *PrimEx* based on the signal size and timing requirements expected. A total of 56 UVA120A modules (36 input, 2 output linear fan-ins) and 4 UVA125A (quad 9 input linear fan-in with discriminator) modules are needed. The power requirements of the UVA120A units are quite modest while those of the UVA125A are somewhat more demanding. UVA has provided *PrimEx* with six high powered NIM crates for use with these modules.

5.1.2 Cabling

The main issue with cabling (external to HYCAL) has been the over 1700 channels of delay cables needed for the HYCAL detectors. Delay cables were constructed using special order RG58 coaxial cable with a CL2 fire rating, non-contaminating jacket, and supplemental foil shield. Approximately 1/2 million feet of cable was purchased for this. The cables were cut to 400 ns lengths. Each channel was tested to be within 2ns of 400ns. The cables were soldered to custom designed printed circuit boards with connectors which could be mated directly to the LRS1881M ADC modules. The HYCAL end used a similar type of mass termination. The delay cables were produced in bundles ranging from 25 to 32 cables each. Work on these cable bundles was completed during the summer of 2003.

5.2 Event Triggers

Several event triggers will function during the taking of production data. These are described in the following sections. The triggers will be implemented using the Trigger Supervisor's ability to accept up to 12 independent triggers.

5.2.1 π^o trigger

The π^o trigger will be the primary trigger for physics events. The electronics basically use information from HYCAL to create a trigger when two clusters exist in the calorimeter. This is done by essentially fanning in strips of detectors 5 or 6 high which span the calorimeter. The strip signals are discriminated on. By having strips which span the entire calorimeter, showers are guaranteed to be at least 50% contained in a single strip. Because the strips are at least 10cm apart, events in which two non-adjacent strips fire would signal two clusters in the calorimeter. This explanation is somewhat simplified since shapes, amplitudes and timing of signals from the lead-glass and PbWO4 differ, preventing one from mixing the two detector types in a single fan-in. Another consideration is that two clusters could occur on opposite sides of the same strip, causing only that strip to fire. This is addressed by replicating the logic, but for strips rotated 90 degrees with respect to the first.

This algorithm is implemented in the electronics in the following way: UVA120A linear fan-in modules housed in crates mounted under the HYCAL will fan-in between 25 and 36 dynode signals from the detectors (see fig. 31). The UVA120A's have two inverted outputs. High speed (0.87c), low-impedance coaxial cables are then used to carry the inverted [1] signals up to the UVA125A modules in the racks on level 2 of the space frame. The UVA125A modules perform a second stage of fan-in and apply a discriminator. The discriminator will see the sum of the entire strip. Discriminator thresholds are set via a front panel DC input. These are in turn, driven by a CAMAC controlled DAC so that the discriminator thresholds can be adjusted from the counting house.

Th π^o trigger will actually be dominated by accidentals from Compton scattering and scattering from the beam pipe upstream of the PS dipole (see section 5.2.6). The rate can be adjusted by either raising the threshold, or lowering the beam current. These will be adjusted so that the π^o trigger rate is about 2kHz.

5.2.2 PS trigger

The purpose of the pair spectrometer trigger is to provide a gate well-timed with the pair spectrometer ADC signals. This will be used to monitor the gains of the paddles. In particular, to monitor the gain's dependence on the rate. The Pair Spectrometer trigger will come from a 4-fold coincidence of the upstream-left/right, downstream-left/right pair spectrometer paddle groups. This trigger has been used successfully in CLAS data taking.

As a special purpose monitoring trigger, the rate of PS triggered events will contribute a small fraction of the total event rate. We plan to prescale the PS trigger so that its rate does not exceed 0.5% of the total trigger rate.

[1] Inverting the dynode signal makes it "right-side-up" i.e a negative going pulse as is expected in the UVA125As

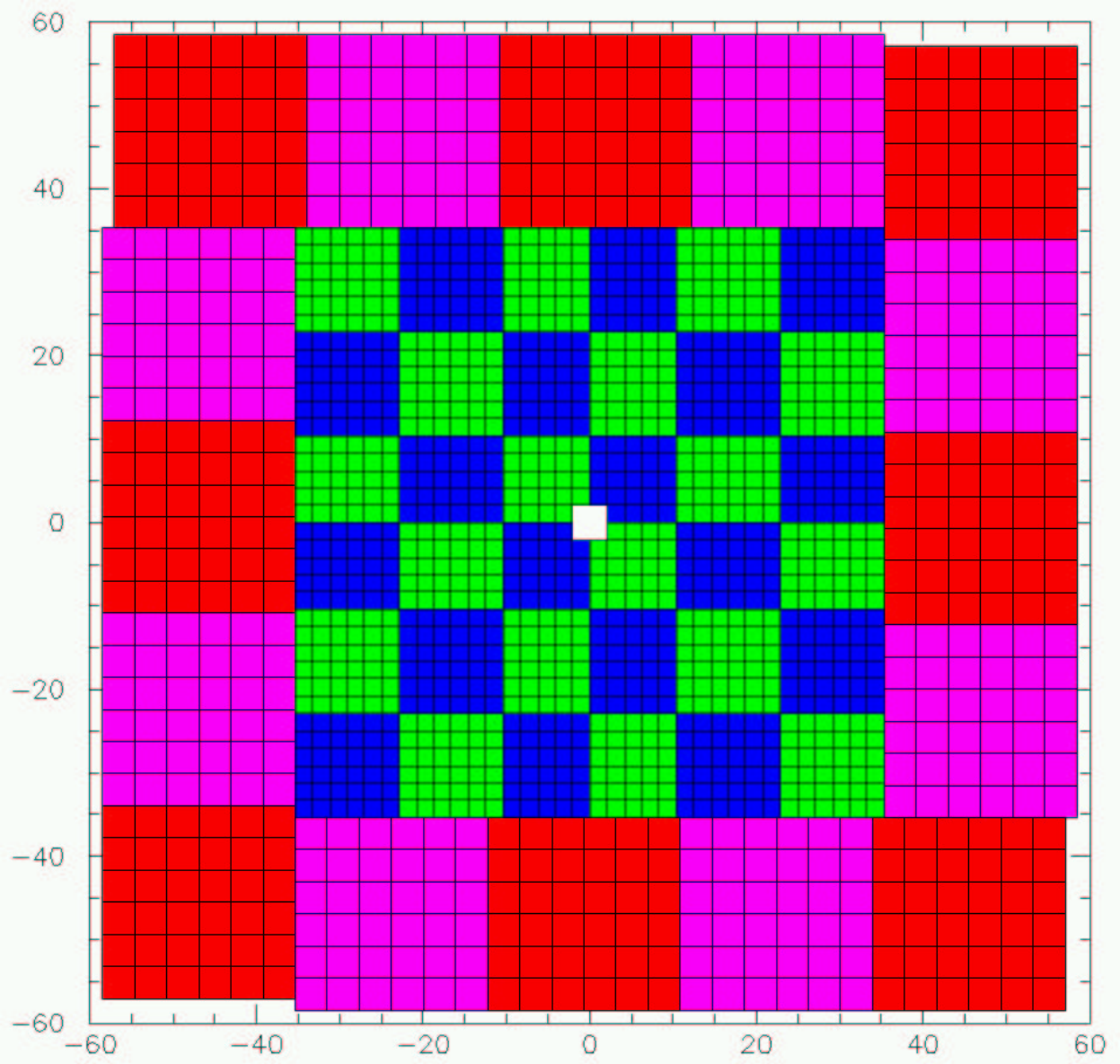

Figure 31: The detector groups formed by the first stage fan-ins.

Trigger	Rate
π^o	2 kHz
PS	10 Hz
LMS	2 Hz
Clock	1 kHz
Total	3kHz

Table 1: Triggers that will be used during *PrimEx* and their anticipated rates during production running.

5.2.3 LMS trigger

The Light Monitoring System trigger will occur whenever the LMS sends a light pulse to the HYCAL detectors. This will be used as a separate trigger which can be individually prescaled so as to give control over the rate from the counting house. One caveat of the LMS is since it will light every detector in HYCAL, it will also cause π^o triggers. To avoid this, the π^0 logic programmed into the MLU modules will not fire when every strip fires as this will be assumed a LMS event.

Another concern of the LMS events is that since every channel is above threshold, all 1728 detectors will be read. The LMS events will therefore contain more than 10 times as much data from HYCAL as π^o events. For this reason, the LMS trigger rate will not exceed 1Hz [2].

5.2.4 Clock (luminosity) trigger

The clock trigger is used for luminosity monitoring. The idea is that we need an unbiased sample of hits in the tagger to measure the average luminosity. In principle, we could use out-of-time events in the π^o triggers, but these are susceptible to higher frequency beam current fluctuations which can be difficult to monitor and even more difficult to correct for. The clock will be produced using a crystal oscillator. A module designed by the Hall-B fast electronics group has been built for *PrimEx* which will provide 10^4, 10^3, 10^2, and 10^1 Hz signals. *PrimEx* will use the the 10kHz trigger prescaled by a factor of 10 using the Trigger Supervisor. This will give us the option of fine tuning the clock trigger rate easily from the counting house.

5.2.5 Trigger Rates

For the August 2002 beam test, the DAQ system was pushed to an event rate of around 6kHz. This corresponded to a fairly low live time of about 20%. For *PrimEx* production running, we will run such that the live time does not fall below 80%. This will correspond to a DAQ rate of approximately 3 kHz. A summary of the *PrimEx* triggers and their anticipated rates is shown in table 5.2.5.

[2]There are preliminary plans for a smarter LMS trigger which will fire at an increased rate (~10Hz) automatically during beam trips.

5.2.6 Monte Carlo Trigger Studies

With the modifications required for the trigger due to the new geometry of HYCAL, a new Monte Carlo study was performed to estimate the acceptance efficiencies and trigger rates. The new study had several improvements over the original including energy smearing, a more accurate beamline definition, more realistic detector geometry, and realistic bremsstrahlung angular distribution.

The first part of the study focused on the trigger's acceptance efficiency for Primakoff π^o events. The programming of the C542 MLU units was emulated in software so that the algorithm could be fully tested. Figure 32 shows the event viewer used to analyze simulated data. The acceptance efficiency is expected to be nearly 100% for π^o decays whose photons each have a given minimum energy (determined by discriminator threshold settings) and have trajectories pointing to the fiducial part of HYCAL. The few trigger failures expected are due to energy leakage through the cracks between detectors in HYCAL. Figure 33 shows a plot of the trigger efficiency *versus.* the minimum decay photon energy if the trigger were set to accept all 500MeV or greater photons. This plot shows that the triggering efficiency is quite insensitive to the discriminator threshold.

The second part of the Monte Carlo study focused on estimating the trigger and detector rates due to backgrounds and accidentals. Figure 34 shows an upper limit of the PrimEx trigger rate as a function of the decay photon energy, estimated by simulation. This upper limit was calculated assuming a 50 ns coincidence window. In reality, PrimEx will use something closer to 20 ns. A "worst case scenario", however, was employed in order to obtain a believable upper limit. An arrow on the plot indicates the 750MeV photon energy point with an event rate of approximately 1.5kHz. Unlike the triggering efficiency, the background rate is very sensitive to the value of the discriminator thresholds. For the actual experiment, the thresholds will be set as low as possible such that the deadtime does not exceed 5%.

The primary contribution to background rates come from two sources: 1.) e+e- pair production upstream of the Helium bag and 2.) Compton scattering from the Helium itself. Figure 35 shows the sources of these backgrounds along the beamline. Backgrounds originating in the beampipe are due to large angle bremsstrahlung photons showering in the beampipe. Occasionally, some energetic shower photons will pass down the beamline, through the magnet, and into HYCAL. These types of events will be easily rejected in software.

Further simulation studies estimated discriminator rates and detector rates. The expected discriminator rates are shown in figure 36 for the $PbWO_4$ detector strips. The rates corresponding to the minimum decay photon energy of 750MeV (initial *PrimEx trigger point*) for the innermost strips will fire at less than 10kHz.

5.3 Data Format and Data Rates

5.3.1 Data Format

PrimEx will use the CODA format for recorded data. The CODA physics events will contain the words as read from the fastbus modules. All decoding will take place offline. The *PrimEx* analysis software has already implemented a library of IO functions to read, write and parse

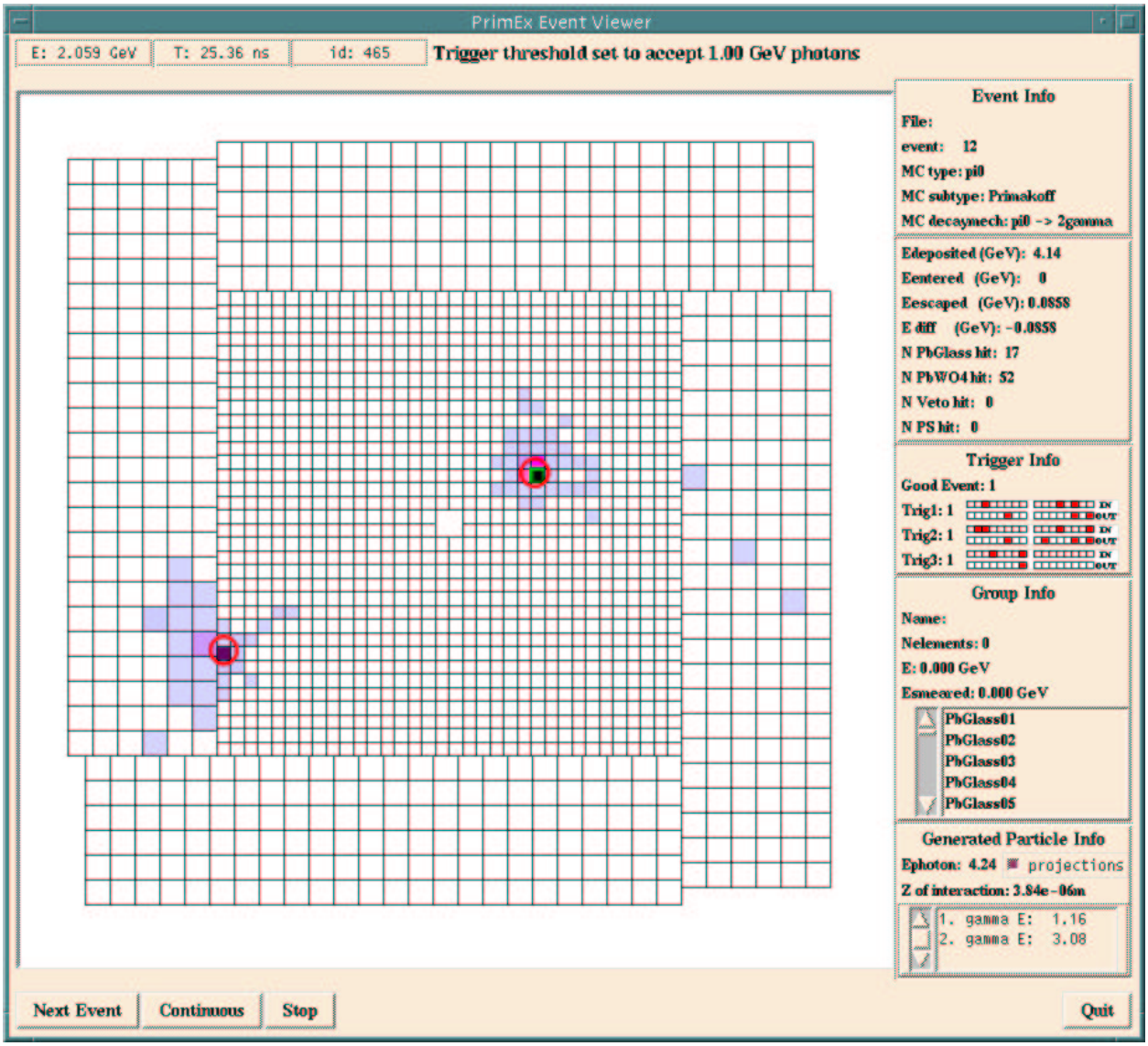

Figure 32: PrimEx event viewer for Monte Carlo data. This is used to diagnose individual events and the trigger's response.

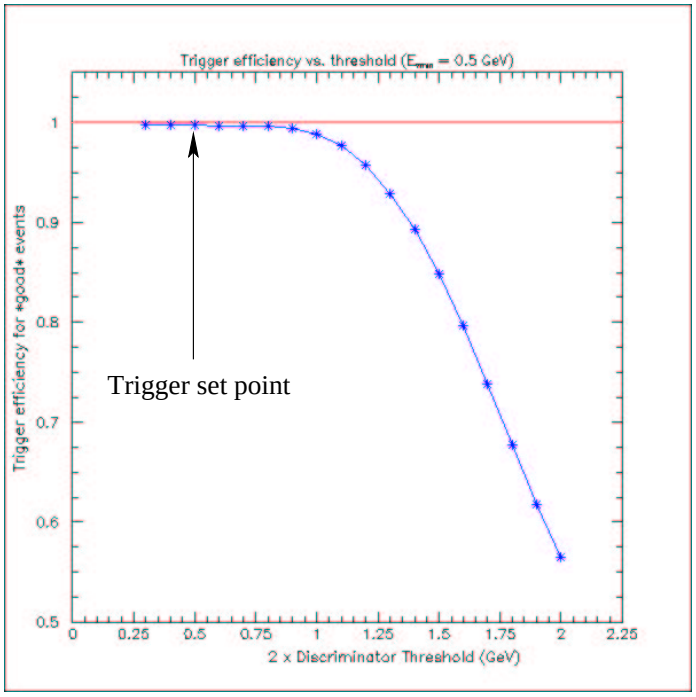

Figure 33: Plot of the trigger acceptance efficiency (estimated from simulation) vs. discriminator threshold. The acceptance efficiency is based on accepting 500MeV or greater photons. The arrow indicates where the threshold should be set for accepting 500MeV photons. The curve shows that the acceptance efficiency is very insensitive to the discriminator threshold.

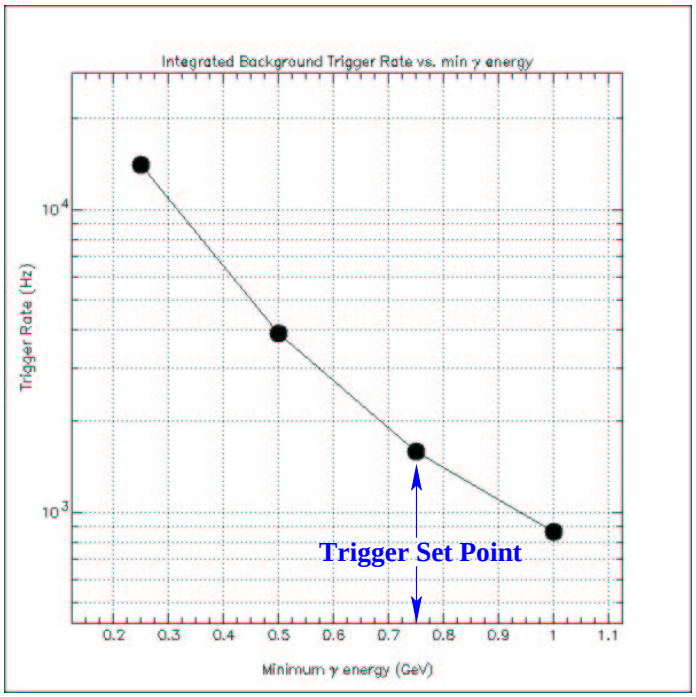

Figure 34: Trigger rate (upper limit) due to background vs. the minimum decay photon energy. The rate includes accidentals from combining several background events. The discriminator values will initially be set to correspond to the 750MeV decay photon energy point. The final discriminator values will be determined by the deadtime in the DAQ system.

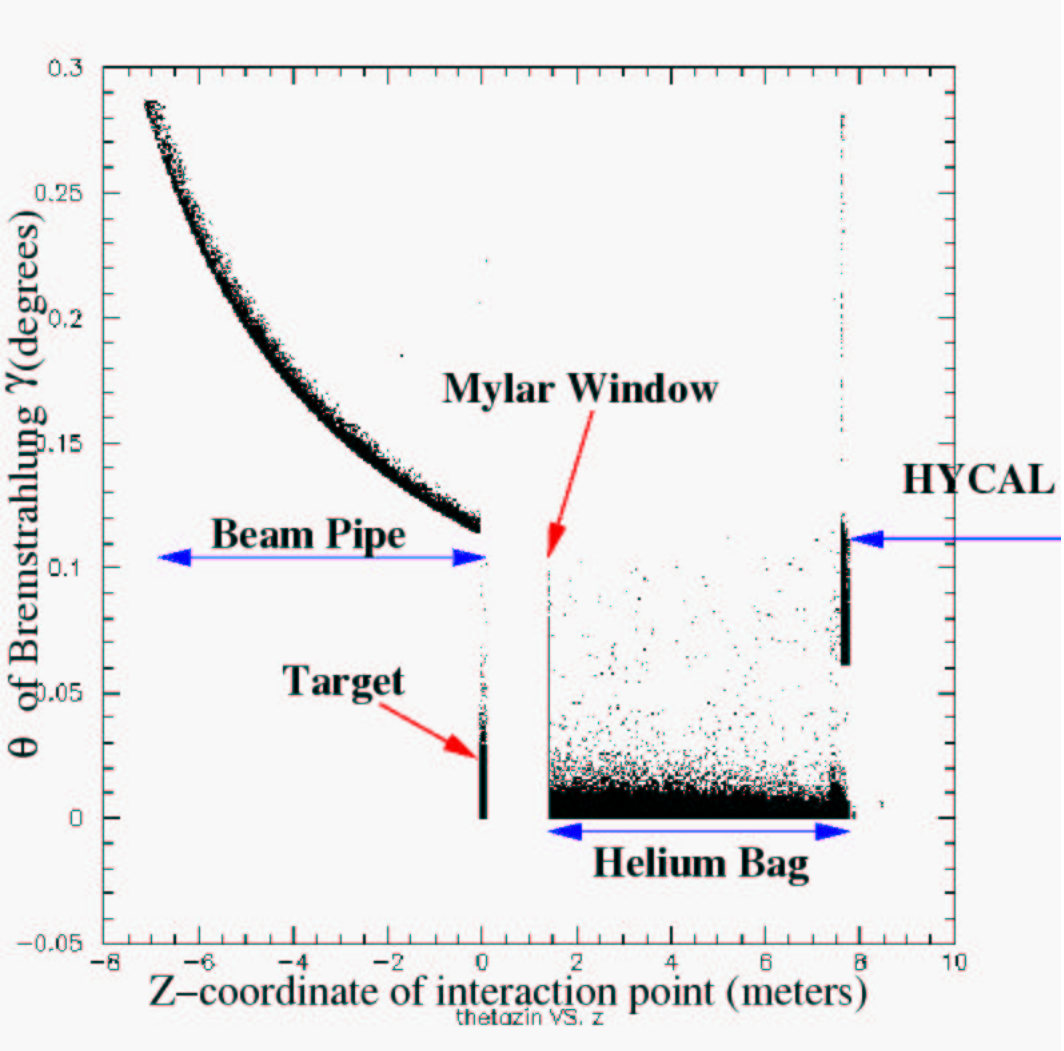

Figure 35: Location of background sources along Hall-B beamline. The angle of the bremsstrahlung generated beam photon is plotted vs. the position along the beamline at which the initial interaction took place. The relevant beamline components included in the simulation are shown.

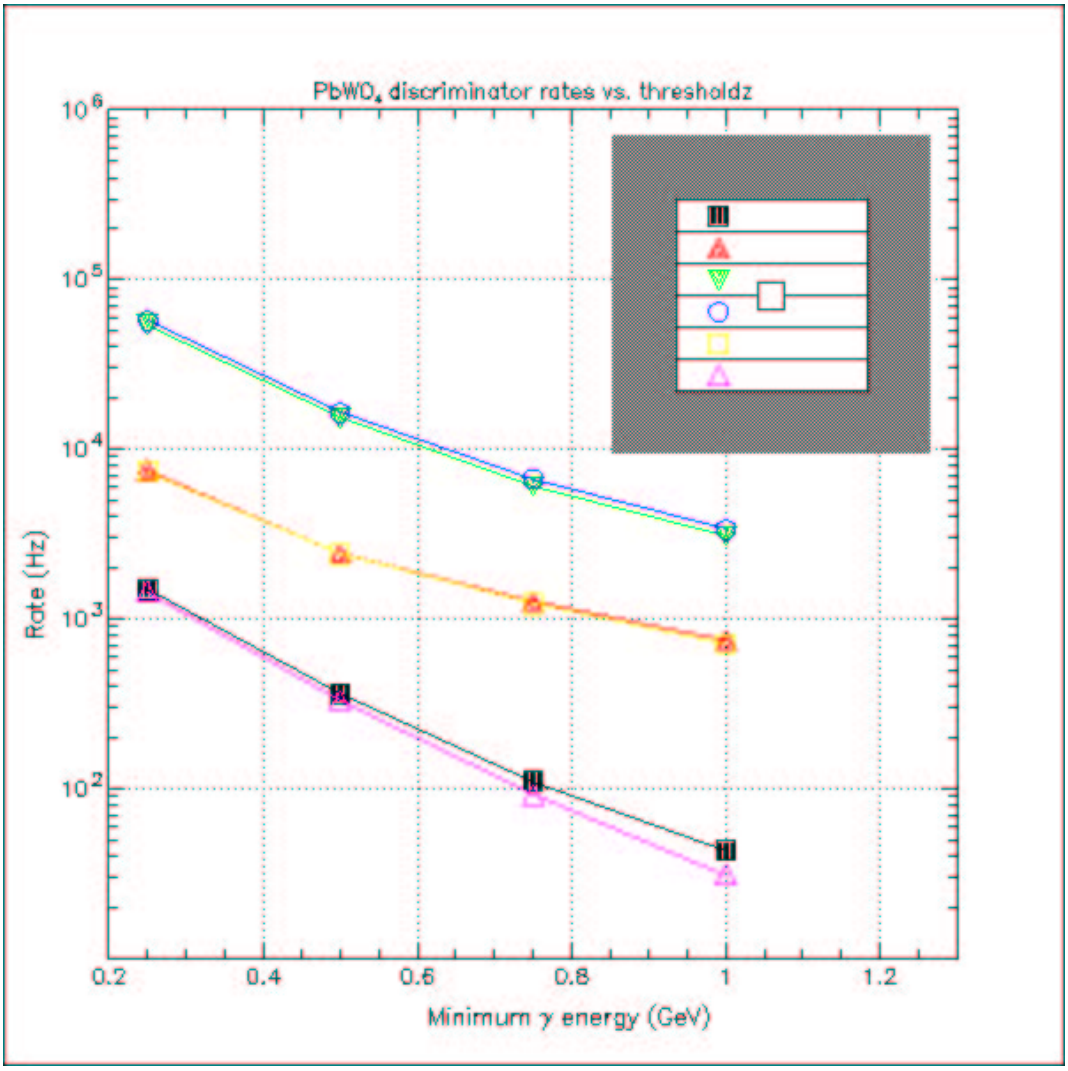

Figure 36: Discriminator rates for different sections of HYCAL based on simulation study.

the CODA formatted files. Additionally, a CODA bank definition has been created to record and read/write *PrimEx* "banks" (see sections 5.4-5.4.2).

5.3.2 Data Rates/Event Sizes

The photon tagger will almost completely dominate the event size. With an average of 1MHz per T-counter and 19 T-counters, we expect a 19MHz rate for the tagger. With a $10\mu s$ TDC window, we expect 190 photons per event. The post-bremsstrahlung electron will hit 1 T-counter and 1 2/3 E-counters on average. This translates to about 6.1MB/sec for an event rate of 3kHz. For the same event rate, HYCAL will provide only about 1.2 MB/sec assuming only 100 detectors pass sparsification per event on average.

5.4 Analysis Software

Considerable development of analysis software has been performed. The modular code is kept under CVS control on the JLab CUE on the primex group disk. The programs have been developed to read the CODA formatted data from HYCAL-0 beam tests in August 2002. This format has also been fully implemented into the simulation code to allow seamless analysis of both real and simulated data. *PrimEx* implemented a calibration database based on the design of the CLAS database using MySQL. There currently exists over 50k lines of *PrimEx* simulation and analysis code in the primex CVS repository.

5.4.1 Object Framework

The *PrimEx* analysis software is built on a framework made of several C++ objects. The important feature is the PEvent_Loop class which implements an event loop which can be used by all programs. Analysis programs typically have main() routines with only 5-10 lines of code. This makes development time of new programs minimal since all common functions are handled by the PEvent_Loop object.

5.4.2 Bank Definitions (BDML)

To facilitate communication between different modules of the primex analysis software, a bank structure was defined. Some properties include standard access mechanisims, dynamic resizing, and extensibility. Top level definitions of the banks was done by creating a flavor of XML dubbed the Bank Definition Markup Language (BDML)[4]. With BDML, a new bank is easily added to a single BDML file and the necessary code is automatically generated by make. Additionally, the bank printing routines and documentation are standardized and generated directly from the BDML source.

5.5 Online Monitoring Software

5.5.1 ET system

The CODA data acquisition system has been integrated with the CEBAF Event Transfer or ET system. This allows one to copy events from the ET system for online analysis without

interrupting the data flow onto disk. The Hall-B counting house has several computers dedicated for online monitoring. *PrimEx* successfully tested an et2et program which copied events from the primary data acquisition computer clon10 to a secondary machine, clon00, where online monitoring programs were run. The analysis software discussed in section 5.4.1 has been written to allow events to be read from an ET system as easily as from a file. This gives *PrimEx* the flexibility to run any program written for offline in an online environment.

5.5.2 Monitoring Programs

A philosophy has been adopted for the *PrimEx* software which is as follows: Each detector system (HYCAL, tagger, pair spectrometer, ...) will have its own library of reconstruction software. In addition, each system will have a program which will satisfy three criteria:

1. Produce plots (histograms, scatter plots, ...) which indicate the system is working properly.
2. Produce plots which enable one to derive calibration constants easily.
3. Produce plots which check the quality of the existing calibration.

It is in this context that a number of programs have been developed for *PrimEx*. These are:

- hycal_calib
- tagger_calib
- ps_calib
- tac_calib
- prim_monitor

These programs will all be run online to both check the functioning of the various detector systems as well as provide a means for quickly calibrating the detectors so that the quality of the data may be monitored as well.

5.5.3 PrimEx Event Viewer (pev)

In addition to the statistical monitors described in the previous section, a graphical single event viewer has been written. The PrimEx Event Viewer or *pev* was written to provide a way of quickly looking at individual events in detail. It has views of the HYCAL, tagger, and Pair Spectrometer. Figure 32 shows a screen shot of an early version of the viewer looking at Monte Carlo data. The event viewer will read events from the ET system on clon04 in the counting house and will be in continuous operation during data taking.

5.6 DAQ and Electronics Summary

- The *PrimEx* experiment will utilize fastbus technology to digitize signals from all of its detector systems (HYCAL, tagger, PS, ...) This equipment was used successfully during the August 2002 beam test.
- The primary physics trigger will be implemented using UVA designed, NIM standard modules (UVA120A and UVA125A). The trigger will occur when two clusters separated by at least 10cm are present in HYCAL. Simulation studies indicate high efficiency with little sensitivity to thresholds.
- All modules and crates are currently on site and are in possession.
- *PrimEx* will take production data with an event rate of approximately 3kHz and an data rate of approximately 7.3MB/sec.
- Over 50k lines of code has already been written for *PrimEx*. Approximately 30k lines of this is specifically for data analysis and online monitoring.

6 Beamline instrumentation

6.1 Electron beam position monitors

There are two cavity electron beam position monitors upstream of the tagger. They are 50 feet apart and have an accuracy of $\pm 50 \mu m$. Their stability depends on the beam current. At 1-2 nA, they are stable to within $\pm 50 \mu m$.

6.2 Harp

A photon harp has been installed just upstream of the *PrimEx* target. It consists of three tungsten wires which are 100μm thick, oriented so that the beam traverses 300μm of tungsten. In addition, three ancillary aluminum targets are mounted on the stick, of thicknesses 10^{-2}, 10^{-3} , and 10^{-4} radiation lengths.

6.3 Online scintillating fiber based position monitor

Downstream of the HYCAL, there will be a scintillating fiber online photon beam position and profile monitor. It will consist of two arrays of 2 mm fibers oriented at 90 degrees to one another for $x - y$ position determination. Each array will have 64 fibers which will be read out from internal amplifier-discriminators. The signals will be sent to scalers which will be read in EPICS at 1 to 2 Hz, providing online monitoring of the centroid and width of the beam. This information will also be in the data stream. Each fiber can be read out at up to 10 MHz. A photo of this detector is shown in figure 37. A similar monitor will be placed in the cave downstream of the CLAS.

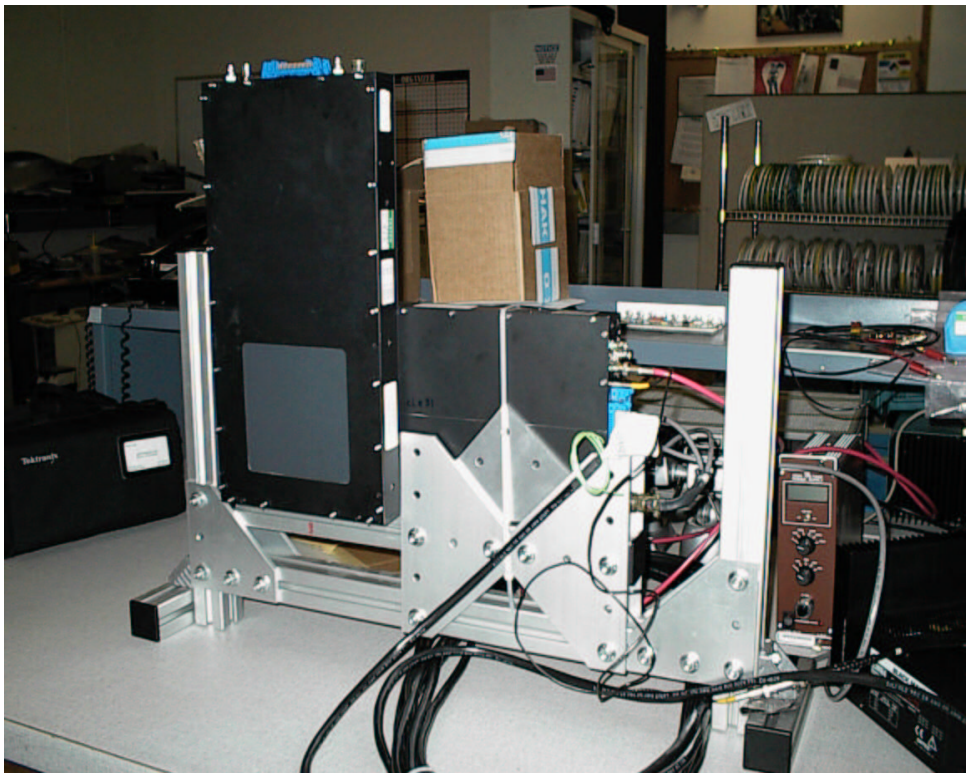

Figure 37: The *PrimEx* scintillating fiber beam position monitor.

6.4 Slow Controls

Below is a list of devices that will be controlled and/or monitored. The status of the work is also mentioned.

1. HyCal transporter: This is epics controlled. The interface software is complete, and was successfully tested in the August 2002 run. A Perl/Tk GUI is being developed and will be available in the coming week. Its task is to set a specific detector module on beam, scan the beam on specified detectors, etc... The motor positions as well as the encoder information will be passed to the data stream. The software for passing epics data to the data stream is ready.

2. HyCal temperature control system: This is Labview controlled. The software was tested during the summer 2001 and 2002 runs. The data from the temperature sensors will be converted to epics data and passed to the data stream. The same will apply to the temperature sensors for the Light Monitoring System.

3. High Voltage control system: This is controlled by a Tcl interface to CAEN Linux libraries. The GUI is ready to use and controls about 1200 channels. Most likely the HV values will be recorded in the data stream at regular time intervals.

4. Target system: This is controlled through epics. A medm GUI was developed to setup the targets. It was tested during the 2002 run. The positions of the two motors that control the motion of the targets will be recorded in the data stream.

5. Pair spectrometer dipole: the NMR probes are read out through epics. We plan to install an additional Hall probe at the center of magnet. The epics software for reading it needs to be developed. The power supply for the magnet is also epics controlled. The software for the degaussing of the dipole is ready and will be tested in the coming week or two.

6. In addition to the above experiment specific controls, we plan of course on using the standard Hall B control system such as the tagger, BCMs, superharp etc..

7 Calibrations via Compton Scattering

Compton scattering in the few GeV energy region provides an important tool for measuring the photon beam energy with high precision (at the sub-percent level). In addition, as this process is understood very well theoretically, Compton scattering also represents an unique way to calibrate the systematic errors of the *PrimEx* setup by measuring Compton differential cross section with the same setup used for the π^0 lifetime experiment.

7.1 Energy Calibration

We having been studying a technique in which the energy of the tagged photon beam is calibrated via the electron Compton scattering near the minimum opening angle. The opening angle ($\psi_{\gamma e} = \theta_\gamma + \theta_e$) between the recoil electron and the scattered photon reaches a minimum in the kinematic region where the partial derivative $\frac{\partial E_\gamma(\psi_{\gamma e},\theta_\gamma)}{\partial \theta_\gamma} = 0$. In this case, the determination of the incident photon energy is independent of the beam direction, $\Delta\alpha$, to first order:

$$E_\gamma(\psi_{\gamma e}, \theta_\gamma + \Delta\alpha) = E_\gamma(\psi_{\gamma e}, \theta_\gamma) + \Delta\alpha \frac{\partial E_\gamma(\psi_{\gamma e}, \theta_\gamma)}{\partial \theta_\gamma} + \Theta(\Delta\alpha^2) \tag{15}$$

When $\frac{\partial E_\gamma(\psi_{\gamma e},\theta_\gamma)}{\partial \theta_\gamma} = 0$, the relation becomes:

$$E_\gamma(\psi_{\gamma e}, \theta_\gamma + \Delta\alpha) = E_\gamma(\psi_{\gamma e}, \theta_\gamma) + \Theta(\Delta\alpha^2) \tag{16}$$

If one selects the Compton events in the region near the minimum opening angle, the energy measurement is not sensitive to the systematic uncertainty of the beam direction. We will therefore determine the absolute photon beam energy by measuring the electron and photon scattering angles near the minimum opening angle with the $PbWO_4$ crystal section of the HYCAL.

We simulated the beam energy measurement for a 2×10^7 equivalent γ/sec beam intensity on a 10^{-3} radiation length ^9Be target for a two day running period. The overlap of two E counters in the photon tagger will provide a $\sim 10^{-3}$ energy bin. The following conditions are included in the calculation:

- initial photon beam energies, E_γ are 4.995, 5.000, 5.005 and 5.010 GeV;

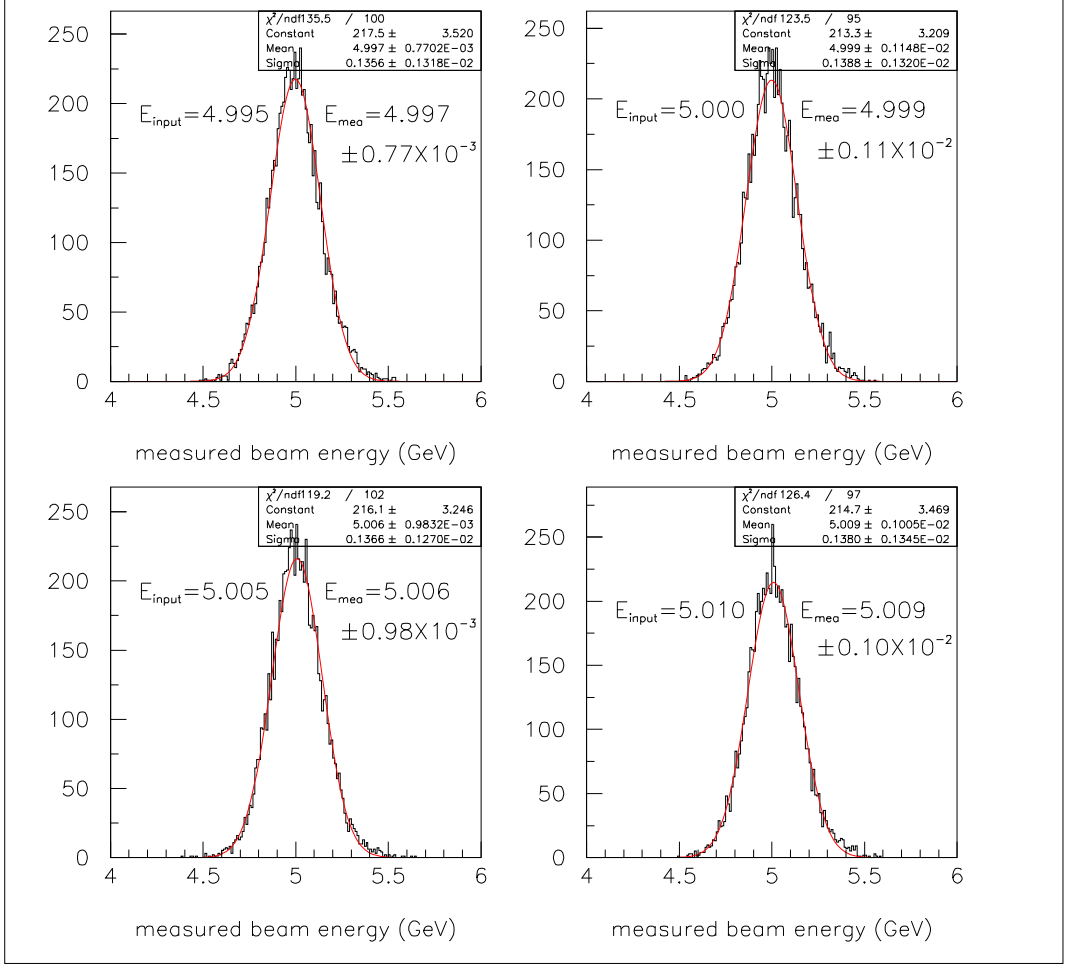

Figure 38: Monte Carlo simulation of the measured beam energy distribution for four different initial beam energies, 4.995, 5.000, 5.005 and 5.010 GeV. The kinematic cuts, $0.4^o < \theta_\gamma < 1.6^o$ and $0.4^o < \theta_e < 1.6^o$, are applied to all plots.

- HYCAL is 9 meters downstream of the target;
- lead tungstate crystal calorimeter resolution;
- multiple scattering on a 0.1% radiation length ^9Be target;
- electron atomic motion effect in ^9Be;
- beam spot size: $\sigma_x = \sigma_y = 0.7$ mm;
- detector misalignment $\Delta x = \Delta y = 1$ mm;
- assumed misalignment of the beam direction: $\theta = 10^{-4}$ rad, $\phi = 0.785$ rad.

Figure 38 shows the Monte Carlo simulations for four different initial beam energies (4.995, 5.000, 5.005 and 5.010 GeV) under the conditions listed above. As one can see, for each step of 0.005 GeV in the initial beam energy shift, the reconstructed beam energy gives the correct answer within the error of $\frac{\Delta E}{E} \sim 10^{-3}$.

7.2 Calibration of PrimEx setup

Electron Compton scattering is one of the simplest and most fundamental reactions in QED. The lowest order Compton scattering diagrams were first calculated by Klein and Nishina in 1929 [11], and by Tamma in 1930 [12]. There are two types of corrections to the basic Klein-Nishina formula which must be considered when studying Compton scattering at energies above 0.1 GeV. These are radiative corrections, and double Compton scattering contributions where one of the final state photons is soft. The interference between the basic first-order single Compton scattering amplitude and the radiative and double Compton scattering amplitudes have been studied extensively in the literature [6]-[8], [9]-[10]. These studies suggest that the higher order corrections to the first-order Klein-Nishina formula would be about $\sim 5\%$ in total cross section [13] when the beam energy is ≥ 1 GeV.

Given the fact that Compton scattering is well understood theoretically, we can measure its differential cross section in the 2.0–5.7 GeV region in the forward angles using the PrimEx setup, which will allow us to study the systematic uncertainties of the setup for π^0 lifetime experiment. The proposed experimental measurements projected to the Klein-Nishina differential cross section are shown in figure 39.

8 Summary

The Collaboration has made significant strides towards getting this experiment ready to run. Some of the major accomplishments at this point are:

- A new Total Absorption Counter (TAC) has been designed and constructed for a high precision determination of the tagger efficiency. The first stage of commissioning with beam has been performed.
- A new harp has been designed, constructed, and commissioned for precise photon beam monitoring.
- Developed a procedure to measure the Primakoff target thicknesses at the 0.7% level and have designed and constructed the PrimEx target ladder.
- Designed, constructed and installed the PrimEx/Hall B Pair Spectrometer for photon flux monitoring at the 1% level.
- HYCAL transporter assembled and in final stages of testing.
- All lead tungstate and lead glass modules assembled and stacked in frame.
- Approximately 2000 high voltage dividers constructed and tested with PMT's.
- Installation of all PMT's in HYCAL complete.
- Cosmic ray tests will start week of December 1^{st} in Test Lab with full *PrimEx* electronics and DAQ.
- Designed and tested a light-based gain monitoring system for the Hybrid Calorimeter.

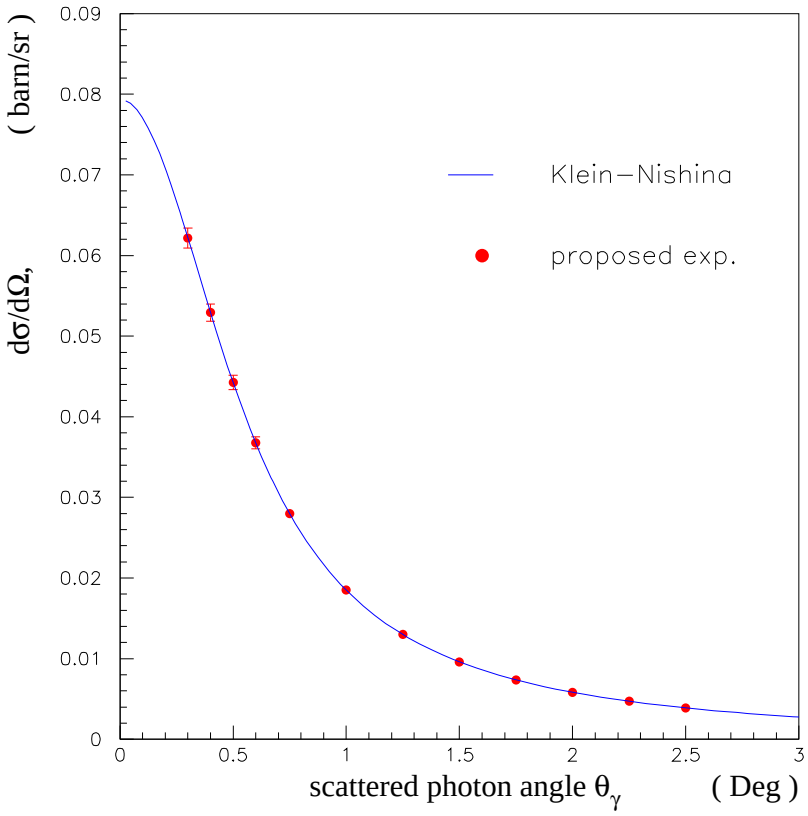

Figure 39: Electron Compton scattering differential cross sections for 5 GeV photon beam. The data points are the proposed experimental measurements projected on to the Klein-Nishina formula.

- Procured veto scintillators for the Hybrid Calorimeter.
- Designed the data acquisition electronics and slow controls systems.
- Refined our studies of trigger efficiencies and backgrounds.

The PrimEx experiment is in full development phase. The experimental setup is planned to be ready for installation in Hall B during the first part of 2003. It is the intention of the Collaboration to run this experiment during the second part of 2003.

9 Appendix I: Engineering

Following is an itemized list of the current status of the engineering for the HYCAL detector and the beamline devices as performed by the Hall B Engineering group.

- **HYCAL Transporter and Motion Controls:**
  - ☐ Major installation in the Hall has been completed.
  - ☐ Load test with a full load of 13,200 lbs. (see figure 40) has been completed. Load tests were done both at the center and off-center positions of the transporter, to allow for torque on the system.
  - ☐ Vertical and horizontal motion systems have been tested with full load pending finalizing the following sub-items:
    - Select and install final limit switches.
    - Install angle transducers.
    - Set the interlocks and finalize the driver software motion control under EPICS.
  - ☐ Cable storage and handling hardware has been installed and ready to be tested.

- **Electronics Deck:**
  - ☐ Structure and lighting of the deck has been completed.
  - ☐ Power for the racks and rack supports have been completed.

- **HYCAL Detector Box/Frame:**
  - ☐ Frame structure has been completed.
  - ☐ Enclosure plates for detector box has been completed pending making thin windows for beam entrance and exit.
  - ☐ Cooling system:
    - 50% of the insulation has been installed.
    - All plumbing hardware is on-hand at JLab and design has been completed. Installation of hardware will be completed by December, 2003.

- **HYCAL In-beam Structure:**
  - ☐ Support cart has been completed.
  - ☐ Alignment cartridges have been completed.

- **Beamline Devices:**
  - ☐ Photon Harp has been completed.
  - ☐ Target Ladder has been completed.
  - ☐ Pair Spectrometer has been completed.
  - ☐ Helium Bag prototype has been fabricated.
  - ☐ Total Absorption Counter and Beam Position Monitor support structure is at the 80% complete design stage.

Figure 40: HYCAL Transporter load test with a full load of 13,200 lbs. performed in Hall B.

10 Appendix II: Technical Details of Pair Spectrometer

10.1 Detectors

The full complement of pair spectrometer detectors required for the PrimEx run (16 telescopes or a total of 32 detectors) is constructed and installed in the Hall. For general use to the Hall B photon physics program, we are presently constructing an additional 16 telescopes to extend the range of photon energies which may be tagged.

Figure 41 shows a side view of a detector module. The front scintillators are $2.4cm \times 7.5cm$ and $0.5cm$ thick, and the rear scintillators are $9.3cm \times 3.1cm$ and $2cm$ thick. The photomultiplier tubes (front detectors: Hamamatsu R6427, rear detectors: R580-17) are shielded from magnetic fields with μ metal, and their voltage dividers have been modified to enable extra power supplies to be applied to the last three dynodes for enhanced high rate capability.

A drawing of the detector assembly is shown in figure 42. The detector mounting system has been designed so as not to interfere with the geometrical acceptance of the HYCAL which is downstream of it, and the amount of material in the median plane of the magnet has been minimized using carbon composite material. A photograph of the detectors and support frame in the Hall is shown in figure 23.

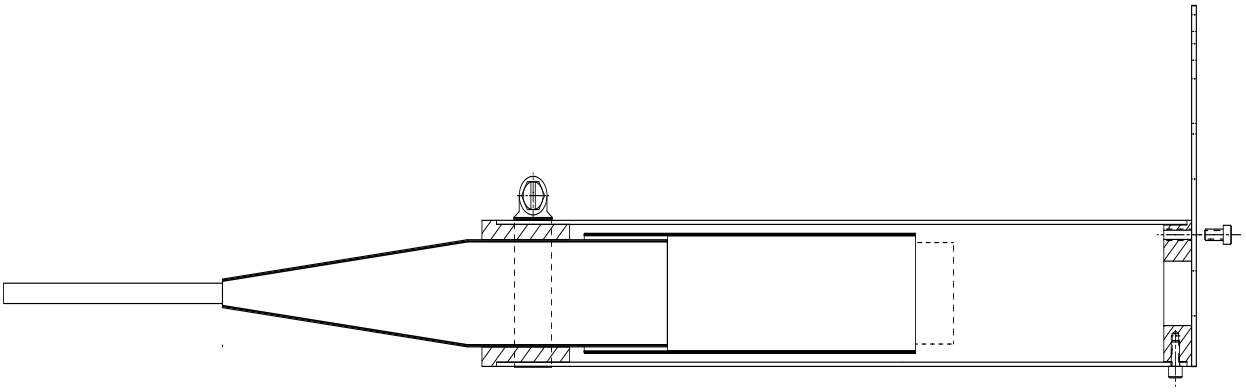

Figure 41: Side view of a front detector module. Scintillator (left, viewed edge-on), light guide (center), and photomultiplier tube (right) are all glued with optical cement. Patch panel for routing cables extends upward on the right.

The pair spectrometer and its associated data acquisition electronics has been installed and commissioned. Preliminary commissioning was done during the $g8$ run in the summer of 2001, and partial commissioning was done in mid-September of 2001. A typical online plateau curve for a detector module, taken with beam, showing singles rates *versus* high voltage is shown in figure 43.

10.2 Results from Magnet Mapping

The PrimEx/Hall B pair spectrometer magnet was mapped in Hall B with the vacuum box in place in May 2001. The mapper consists of a motorized moving cart holding three Hall probes, one on top of each other, in order to map three planes simultaneously. Three motors ensure the backward-forward and the horizontal motion of the cart. Three high-precision (25 μm) encoders were used to determine the position of the cart and hence of the probes. A NMR magnetic probe is used as a reference for the three Hall probes. The mapper is completely computer-controlled. The motion of the cart and the reading of the Hall probes is controlled through epics. The mapper was fully tested in late April 2001. A picture of the apparatus is shown in figure 44.

The principal achievements of these measurements are:

- The procedure to set up the field was established.
- The excitation curve (central field *versus* current) was measured with an NMR probe.
- Full maps were obtained at 0.5, 0.9, 1.0, 1.3, 1.5, and 1.6 Tesla.

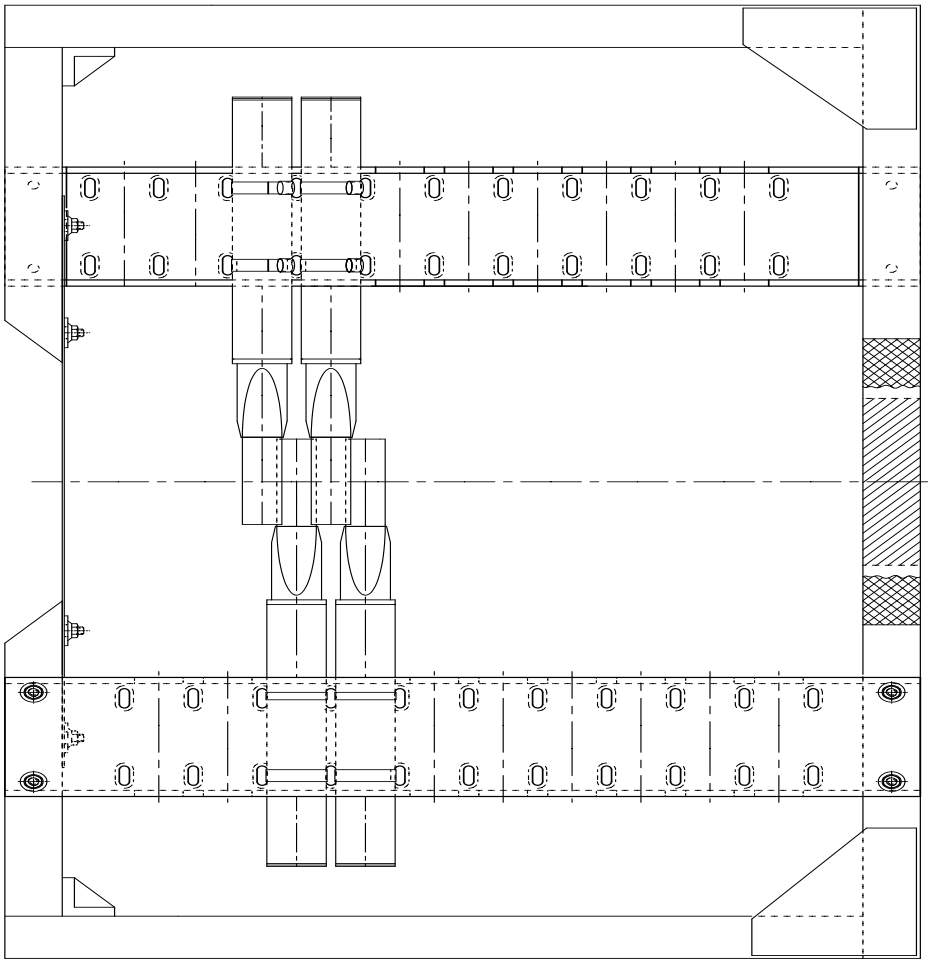

Figure 42: The pair spectrometer detector support frame, with four detectors shown mounted.

- Central line fields were measured from 0.2 to 1.8 Tesla in 0.2 T steps.
- An automated degaussing procedure has been developed for the magnet.

The $\int Bdl$ was determined to better than 0.1%. An example of one such map is shown in figure 45, which was obtained at a central field of 1 Tesla.

References

[1] Available at the PrimEx web site: http://www.jlab.org/primex/

[2] Compact Muon Solenoid Technical Proposal, CERN/LHCC 94-38, LHCC/P1, (1994).

[3] R.Y. Zhu, et. al. IEEE Transactions on Nuclear Science, v.45, no.3,(1998).

[4] PrimEx Note 17: *The PrimEx Bank Definition Markup Language*
http : //www.jlab.org/primex/primex_notes/primex_notes.html

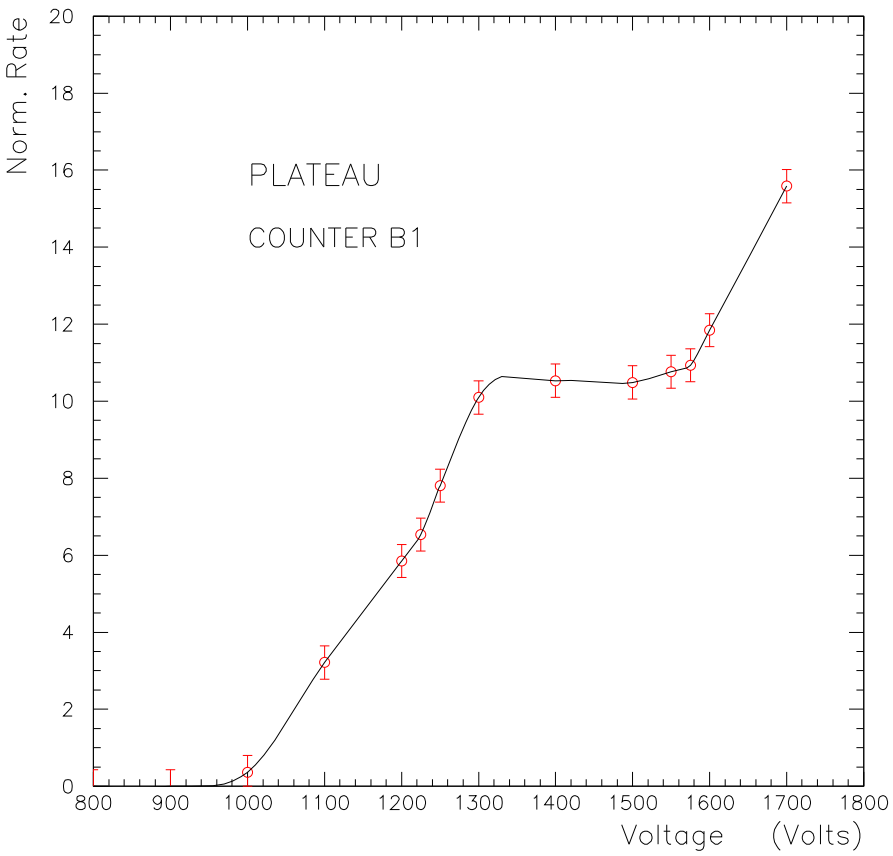

Figure 43: Typical online high voltage plateau curve for a pair spectrometer detector.

[5] A. H. Compton, Bull. Natl. Res. Counc. (U.S) 20, 19 (1922); *Phys. Rev.*, **21**, 483 (1923).

[6] I.M. Brown and R.P. Feynaman, *Phys. Rev.*, **85**, 231(1952).

[7] Till B. Anders, *Nucl. Phys.*, **87**, 721 (1967).

[8] K.J. Mork, *Phys. Rev.*, **A4**, 917 (1971).

[9] F. Mfandl and T.H.R. Skyrme, *Proc. R. Soc. London*, **A215**, 497 (1952).

[10] M. Ram and P.Y. Wang, *Phys. Rev. Lett.*, **26**, 476 (1971); *ibid.* **26**, 1210(E) (1971).

[11] O. Klein and Y. Nishina, *Z. Phys.*, **52**, 853 (1929).

[12] I. Tamm, *Z. Phys.*, **62**, 545 (1930).

[13] A.T. Goshaw et. al.,*Phys. Rev.*, **D18**, 1351 (1978).

[14] Dolgopolov, *et al.*, IHEP preprint 98-25, (1998).

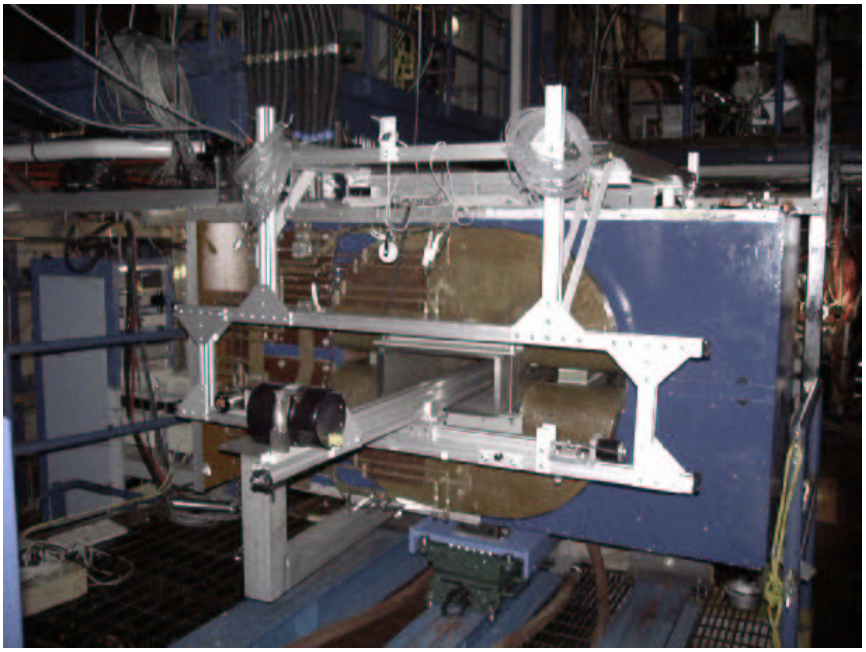

Figure 44: The PrimEx/Hall B pair spectrometer being mapped in the Hall. View is from the upstream side of the magnet looking downstream

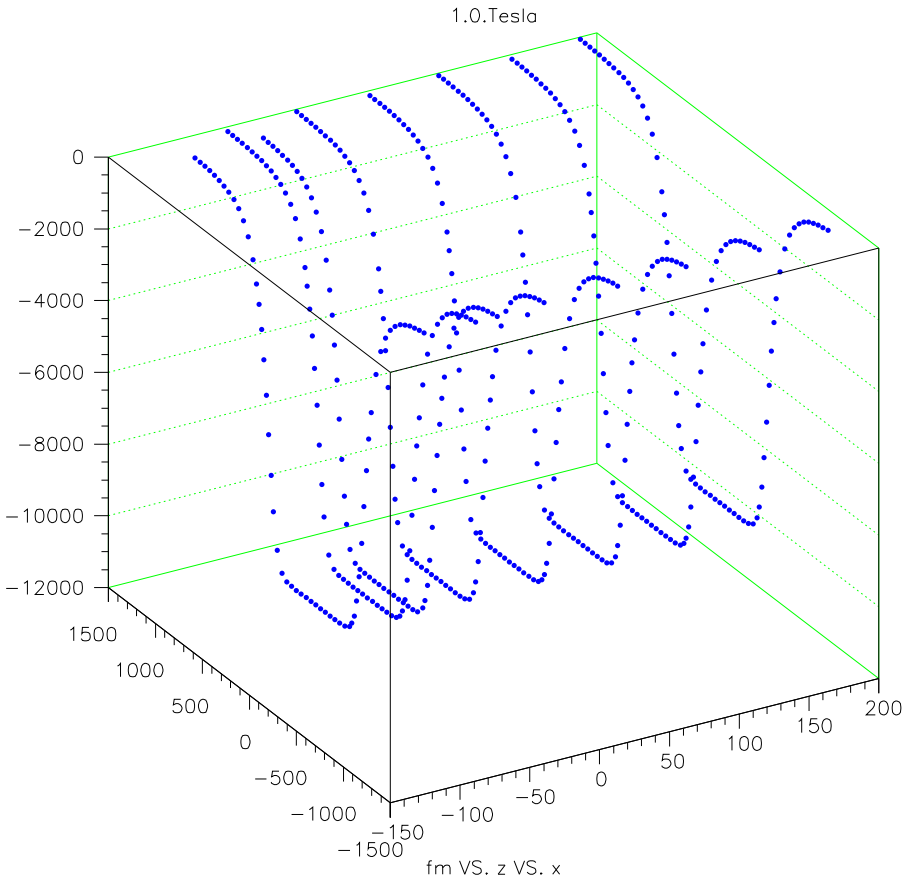

Figure 45: Field map of the PrimEx/Hall B pair spectrometer dipole at a central field of 1 Tesla.